UC Irvine
UC Irvine Previously Published Works

Title
Neuroligin-2-derived peptide-covered polyamidoamine-based (PAMAM) dendrimers enhance pancreatic β-cells' proliferation and functions

Permalink
https://escholarship.org/uc/item/4h42859p

Journal
RSC Medicinal Chemistry, 10(2)

ISSN
2040-2503

Authors
Munder, Anna
Moskovitz, Yoni
Meir, Aviv
et al.

Publication Date
2019-02-20

DOI
10.1039/c8md00419f

Peer reviewed

eScholarship.org Powered by the California Digital Library
University of California

MedChemComm

RESEARCH ARTICLE

View Article Online
View Journal | View Issue

Check for updates

Cite this: *Med. Chem. Commun.*, 2019, **10**, 280

Neuroligin-2-derived peptide-covered polyamidoamine-based (PAMAM) dendrimers enhance pancreatic β-cells' proliferation and functions†

Anna Munder,[a] Yoni Moskovitz,[a] Aviv Meir,[a] Shirin Kahremany,[ab] Laura Levy,[a] Michal Kolitz-Domb,[a] Guy Cohen,[c] Efrat Shtriker,[a] Olga Viskind,[a] Jean-Paul Lellouche,[ad] Hanoch Senderowitz,[a] Steven D. Chessler,[e] Edward E. Korshin,[a] Sharon Ruthstein *[a] and Arie Gruzman *[a]

Pancreatic β-cell membranes and presynaptic areas of neurons contain analogous protein complexes that control the secretion of bioactive molecules. These complexes include the neuroligins (NLs) and their binding partners, the neurexins (NXs). It has been recently reported that both insulin secretion and the proliferation rates of β-cells increase when cells are co-cultured with full-length NL-2 clusters. The pharmacological use of full-length protein is always problematic due to its unfavorable pharmacokinetic properties. Thus, NL-2-derived short peptide was conjugated to the surface of polyamidoamine-based (PAMAM) dendrimers. This nanoscale composite improved β-cell functions in terms of the rate of proliferation, glucose-stimulated insulin secretion (GSIS), and functional maturation. This functionalized dendrimer also protected β-cells under cellular stress conditions. In addition, various novel peptidomimetic scaffolds of NL-2-derived peptide were designed, synthesized, and conjugated to the surface of PAMAM in order to increase the biostability of the conjugates. However, after being covered by peptidomimetics, PAMAM dendrimers were inactive. Thus, the original peptide-based PAMAM dendrimer is a leading compound for continued research that might provide a unique starting point for designing an innovative class of anti-diabetic therapeutics that possess a unique mode of action.

Received 28th August 2018,
Accepted 11th December 2018

DOI: 10.1039/c8md00419f

rsc.li/medchemcomm

Published on 13 December 2018. Downloaded by Bar Ilan University on 2/21/2019 4:40:40 AM.

Introduction

Type 2 diabetes mellitus (T2DM) is reaching catastrophic numbers in human populations and causing high morbidity and mortality due to its severe complications.[1–3] One of the most important pathophysiological components in T2DM is the peripheral tissues' insulin resistance, which in turn leads to increased efforts of β-cells to secrete more than physiological amounts of insulin.[4,5] This chronic overstimulation of β-cells occurs because of futile efforts to compensate for the lack of insulin activity. This overstimulation, in turn, causes β-cell dysfunction. At the beginning of the disease, decreased numbers of normal functioning β-cells are usually detected in the pancreas.[6] Thus, preservation or even augmentation of functional pancreatic β-cell mass is one of the main goals of therapeutic development for T2DM.[7,8] In addition, successful transplantation of β-cells/islets is dependent on a sufficient amount of functioning β-cells.[9,10] Thus, recent scientific efforts have focused on identifying new strategies, which will be able to positively influence β-cell function and/or proliferation and thereby prevent or delay the onset of the disease and its late complications.[11–13] Several β-cell mass protective approaches have been recently developed. This includes, for example, the use of H_2S, which protects cells from apoptosis induced by high glucose,[14] targeting mitochondrial DNA,[15] developing compounds that protect cells under ER stress-induced autophagy,[16] and many others.[17,18]

Regarding T1DM, which is also a life-threatening disease, causing severe complications and increased mortality, there is similarly a need for ways to protect β-cell mass.[19–22] In this

[a] *Department of Chemistry, Faculty of Exact Sciences, Bar-Ilan University, Ramat-Gan, Israel. E-mail: sharon.ruthstein@biu.ac.il, gruzmaa@biu.ac.il*
[b] *Department of Pharmacology, Cleveland Center for Membrane and Structural Biology, School of Medicine, Case Western Reserve University, Cleveland, OH, USA*
[c] *Skin Research Institute, Dead Sea and Arava Research Center, Masada, Israel*
[d] *Nanomaterials Research Center, Institute of Nanotechnology & Advanced Materials (BINA), Bar-Ilan University, Ramat-Gan, Israel*
[e] *Division of Endocrinology, Diabetes & Metabolism, Department of Medicine, University of California, Irvine, CA, USA*

† Electronic supplementary information (ESI) available: Experimental details of the synthetic pathways, synthetic procedures, and analytical data of the synthesized compounds are available. See DOI: 10.1039/c8md00419f

This journal is © The Royal Society of Chemistry 2019

Published on 13 December 2018. Downloaded by Bar Ilan University on 2/21/2019 4:40:40 AM.

autoimmune disease, patients lose the vast majority of their β-cells owing to an aberrant immune attack.[23] The main challenge in T1DM is to protect the remaining β-cells, or, in the ideal case, to even induce β-cell regeneration. To date, only immunosuppressive therapies that begin early after T1DM onset have been able to slightly slow β-cell degeneration and death.[24,25] Together with immunosuppression, autoantigen therapy and agents that can facilitate β-cell regeneration might also be possible drug development options.[26] Because of the huge therapeutic potential in both types of diabetes, the search for novel approaches for preserving or even increasing the β-cell mass has always been very intense.

We recently reported that the HSA-28 peptide, which was derived from NL-2 and covalently attached to the surface of ytterbium(III) cation-doped maghemite nanoparticles (NPs), improved β-cell functionality.[27] The peptide was selected based on the interfacial residues that seem to dominate the interactions between NL-2 and its binding partner neurexin (NX), and which are also completely preserved in the corresponding NL-2 sequence. The rationale to use NL-2 as a basis for developing protective β-cell therapeutics was based on the fact that the secretory/cell contact machinery of the β-cells is similar to that of neurons.[28–31] One of the interacting protein pairs (NLs and NXs) was targeted because of its role in establishing the normal β-cell functioning brought about by β-cell clustering.[28–31] We hypothesized that β-cells treated with NL-2 mimetics might be more functionalized and protected after transplantation.

Indeed, HSA-28-covered maghemite NPs increased proliferation, resistance to oxidative stress, and insulin secretion in both *in vitro* (INS-1E cells) and *ex vivo* (mouse islets) models.[27] However, HSA-28-covered ytterbium(III) maghemite (γ-Fe_2O_3)-based nanoparticles might be not suitable for use in humans, because of genotoxicity[32,33] and neurobehavioral impairments.[34] Herein, our aim was to improve peptide-based cluster functions by using another core platform. Thus, different types of functionalizing NPs were synthesized by conjugation between HSA-28 and the surface amines of a commercially available PAMAM dendrimer. Dendrimers have three-dimensional, highly branched unique polymeric architectures (classically 5000–500 000 g mol^{-1}) and have the benefits of a low polydispersity index, controlled biodegradability, biocompatibility, and the presence of various terminal multivalent functional groups on their surface.[35] Dendrimers are widely used in nanomedicine as potential carriers for various drugs, bioactive molecules, and genes.[36,37] The prepared HSA-28D (HSA-28-coated PAMAM) improved β-cell functions in terms of the rate of proliferation, glucose-stimulated insulin secretion (GSIS), cell maturation, and insulin accumulation. In addition, this functionalized dendrimer protected β-cells under stressful conditions that exist in diabetes: oxidative and ER stress.

Peptides play a variety of important roles in biological systems and are also used as therapeutic agents.[38–42] However, the use of peptides as drugs is limited because of several pharmacokinetic disadvantages (for example, protease-induced degradation).[43–45] Although *in vitro* biological evaluation of HSA-28D showed promising results, we tried to take this project even further; various novel peptidomimetic scaffolds of HSA-28 were designed, synthesized, and conjugated to the surface of PAMAM. Peptidomimetics are compounds whose chemical moieties mimic the 3D structure of natural peptides and retain the ability to bind to biological targets, but without the disadvantages of peptides.[46–49] However, covered by peptidomimetics, PAMAM dendrimers were inactive in the proliferation screening assay. Thus, in this work, synthesis of peptidomimetics was used only for developing new organic scaffolds that might be used for the mimicking of glutamic, phenylalanine, and leucine amino acids containing peptides (as it was in our case). HSA-28-based PAMAM dendrimers are leading compounds for upcoming work that might reveal an innovative class of antidiabetic therapeutics that possess a unique mode of action: increasing β-cell mass and functionality *via* targeting its neuronal secretory and adhesion machinery.

Methods

Materials

PAMAM dendrimer (ethylenediamine core, fifth generation), bovine serum albumin (BSA), glucose oxidase (GO), thapsigargin (Tg), protease inhibitor cocktail, radioimmunoprecipitation assay buffer (RIPA), Rink amide resin, 2,2-diphenylethylamine, benzhydrylamine, phenethylamine, benzylamine, glycinamide hydrochloride, α- and β-naphthaldehyde, 1,2,3,4-tetraisoquinoline, *n*-bromoethylphthalimide, potassium carbonate, potassium iodide, *tert*-butyl acrylate, isobutylamine, triethylamine, 2-iminothiolane, and 3-maleimidopropionic acid were purchased from Sigma-Aldrich (Merck) (Rehovot, Israel). Fetal calf serum (FCS), phosphate buffered saline (PBS), L-glutamine, trypan blue, Roswell Park Memorial Institute medium (RPMI-1640), and antibiotics were purchased from Biological Industries (Beth-Haemek, Israel). Formaldehyde (4% in PBS) was purchased from Bio-Lab (Jerusalem, Israel). Rink amide resin, DIEA, and protected amino acids were obtained from Chem Impex (Wood Dale, IL, USA). β-Mercaptoethanol was purchased from Bio-Rad (Hercules, CA, USA). Alfa Aesar (Ward Hill, MA, USA) supplied *t*-isopropanol-silane. Alexa Fluor 633 Phalloidin was purchased from Life Technologies (Carlsbad, CA, USA). Anti-glucagon, anti-C-peptide, and anti-Pdx1 antibodies were supplied by Abcam (Cambridge, MA, USA). The Mercodia Insulin ELISA kit was purchased from Mercodia (Uppsala, Sweden). All organic solvents were purchased from Carlo Erba Reagents (Val De Reuil, France).

Peptide synthesis

The synthesis was performed as described in the literature.[50] The obtained peptide was coupled with 3-maleimidopropionic acid by the N-termini of the peptide according to the peptide synthesis procedure.

Published on 13 December 2018. Downloaded by Bar Ilan University on 2/21/2019 4:40:40 AM.

HPLC purification

Preparative HPLC (Young Lin Instruments, Anyang, Korea) was performed on a LUNA C18 preparative column (10 μm, 100 × 30 mm) from Phenomenex, Inc. (Torrance, CA, USA). Compounds were purified using an increasing linear gradient of acetonitrile in DDW at room temperature.

Peptide conjugation onto the surface of PAMAM dendrimer

Two hundred μL of PAMAM dendrimer in methanol solution (which corresponds to 0.01 g of PAMAM dendrimer) was used for preparing each sample. First, the methanol was evaporated under reduced pressure and the dendrimer was dissolved in 0.5 ml of PBS. Then the solution of dendrimer was treated with a 2-fold excess of 2-iminothiolane (from 0.1 M stock solution of 2-iminothiolane in PBS). After having been shaken for 5 min, a 5-fold excess of HSA-28 peptide or mimetics in PBS was added to the solution above, up to 2 ml of the total volume. The reaction mixture was shaken overnight at room temperature.

The coated NPs were purified using a centrifuge ultrafiltration system (3000 rpm, 20 min, 10 °C, 3 times) until the filtrate did not contain any traces of the compound (monitoring by TLC under UV light or under vanillin stain).

Cell line

INS-1E β-cells were courtesy of Prof. Shlomo Sasson (Faculty of Medicine, Hebrew University of Jerusalem, Jerusalem, Israel). Cells were grown and maintained as described by Pasternak *et al.*[51]

Cell counting (trypan blue exclusion assay)

Cells were detached by trypsin and mounted using trypan blue (0.4%). Only uncolored cells were counted (live cells). Cell counting proceeded according to the Abcam (Cambridge, MA, USA) online protocol for work with a hemocytometer.

MTT cell viability assay

Cells were incubated with 3-(4,5-dimethylthiazol-2-yl)-2,5-diphenyltetrazolium bromide reagent (MTT, 2 mg ml^{-1}) in growth medium for 2 h at 37 ° C. The medium was then aspirated, and DMSO was added to solubilize the cells and colored crystals. Absorbance at 570 nm was measured in a SpectraMax M5 spectrophotometer (Sunnyvale, CA, USA).

Induction of oxidative stress

Oxidative stress conditions[52] were induced by supplying glucose oxidase (GO, 50 mU ml^{-1}) to the growing medium of the INS-1E cells. This resulted in an elevated H_2O_2 concentration in the medium (reaching 29.0 ± 9.6 μM after 4 h of incubation). The standard MTT cell viability test was performed after 4 h of incubation.

Induction of ER stress

ER stress conditions were induced by supplying thapsigargin (Tg, 0.75 μM) to the growing medium of the INS-1E cells.[53] The standard MTT test was performed after 24 h of incubation.

Immunofluorescence measurement of C-peptide, glucagon and Pdx1 level

Experiments were conducted in INS-1E cells that were seeded on coverslips in 6-well plates. The cells were incubated with HSA-28D for 72 h (control cells were untreated). Following incubation, the slides were washed three times with prewarmed PBS and fixed with formaldehyde (4% in PBS). Subsequently, the slides were washed three more times with prewarmed PBS. The level of C-peptide was determined by immunocytochemistry using anti-C-peptide antibody according to the manufacturer's protocol. The membranes were stained with Alexa Fluor 633 Phalloidin according to the manufacturer's protocol. The slides were washed three times with prewarmed PBS. Nuclei were stained with DAPI according to the manufacturer's protocol. Fluorescent signals were visualized with a confocal-Zeiss microscope equipped with a 60×/1.4 objective (Oberkochen, Germany). For the glucagon measurement, cells were grown as described above. Slides were incubated with HSA-28D (control cells were untreated) for 72 h. The level of glucagon was determined by immunocytochemistry using anti-glucagon antibody. Thereafter, the slides were fixed with formaldehyde as described above. Cell membranes and nuclei were stained as previously described. Visualization of fluorescent signals proceeded as described above. For Pdx1 level identification, cells were grown as described above. Slides were incubated with HSA-28D for 72 h. The level of PDX1 was determined by immunocytochemistry using anti-PDX1 antibody. Thereafter, the slides were fixed with formaldehyde as described above. Cell membranes and nuclei were stained as previously described. Visualization of fluorescent signals proceeded as described above.

GSIS and insulin content assays

The assays were performed on INS-1E cells as described.[54] Insulin quantification was performed using the Mercodia Insulin ELISA kit according to the manufacturer's protocol.

The pharmacophore design

The pharmacophore was designed based on the structure of HSA-28 peptide and NX-1 using LigandScout 4.0 software.[55]

Synthesis of HSA-28 mimetics

The compounds were obtained by a reaction between commercially available or synthesized *in house* aromatic amines and *tert*-butyl acrylate as described by Ingallinella *et al.*[56] The detailed synthesis procedures are presented in the ESI.†

 This journal is © The Royal Society of Chemistry 2019

Published on 13 December 2018. Downloaded by Bar Ilan University on 2/21/2019 4:40:40 AM.

HSA-28 mimetic conjugation onto the surface of the PAMAM dendrimer

3-Maleimidopropionic acid was coupled to all the synthesized compounds above according to the procedure described by Ruzza *et al.*[57] The coupling reaction was followed by the treatment of all compounds with neat TFA for 1 h as described in the literature. The conjugation of all compounds onto the surface of PAMAM dendrimer was performed as described before.

Estimation of the dendrimer coating by HAS-28D and its peptidomimetics

Polyacryl gel electrophoresis (PAGE). For estimating the percentage of dendrimer coating the gel electrophoresis of the peptide or peptidomimetics conjugated to dendrimers was determined. In addition, as a negative control, we evaluated the electrophoresis of PAMAM that was coated only by 3-maleimidopropionic acid and PAMAM alone. All samples were loaded to glycine using 6% SDS PAGE gel and run against Tris-Tricine-SDS (TTS) running buffer and stained using silver stain.

Gel permeation chromatography (GPC). The molecular weight and polydispersity index (PDI) were determined using gel permeation chromatography (GPC) consisting of a Waters Spectra Series P100 isocratic HPLC pump with an ERMA ERC-7510 refractive index detector and a Rheodyne (Cotati, CA) injection valve with a 20 μL loop (Waters, MA). The samples were eluted with super-pure HPLC water through a linear BioSep SEC-s-3000 column (Phenomenex) at a flow rate of 1 mL min^{-1}. The molecular weight was determined relative to poly(ethylene glycol) standards (Polymer Standards Service-USA, Silver Spring, MD, USA) with a molecular weight range of 100–450 000 Da, human serum albumin (67 kDa, Sigma Aldrich), and bovine plasma fibrinogen (340 kDa, Sigma Aldrich), using Clarity chromatography software.

UV spectroscopy

An Agilent Cary 300 UV-vis spectrophotometer with a slit of 4 nm and a scan speed of 400 nm min^{-1} was used for the measurements. The absorbance measurements were performed at pH 7.4 by keeping the concentration of the samples at 0.175 mM in 1 cm quartz cuvettes. The wavelength ranged from 250 to 500 nm.

Results

Conjugation of HSA-28 peptide onto the surface of PAMAM and estimation of the percentage of coating

The HSA-28 peptide was synthesized as described in the Methods section with an amide moiety on its C-terminal and a maleimide moiety on its N-terminal (Scheme 1). PAMAM dendrimer (fifth generation) with an ethylene diamine core and 128 amino groups available for reaction was chosen for evaluating the peptide assembling because of its size similarity to previously active maghemite nanoparticles (5.4 nm).[27] The conjugation was performed using a known quick single-step reaction involving maleimido-derivatized HSA-28 peptide (Scheme 2).[58] The coated dendrimer (HSA-28D) was purified by centrifuge ultrafiltration until the filtrate did not show any traces of starting materials (monitoring by TLC, followed by vanillin staining).

For estimating the percentage of dendrimer coating, 6% SDS PAGE was performed in TTS (Fig. 1A). As expected, the coated nanoparticles appeared as a broad band at around 50 kDa, which corresponded to approximately 21 units of peptide that was conjugated to the PAMAM. Based on this information, the calculated percentage of the covering was approximately 16%.

In addition, the GPC analysis of HSA-28D revealed a single peak at 47 kDa, compared to the calibration curve. This peak has a PDI value of 1.0029, calculated by MW/Mn, where MW is the weight's average molecular weight and Mn is the number's average molecular weight. This indicates the purity of HSA-28D, due to the clear homogeneity seen in the GPC analysis. This result is also well correlated with the result provided by the Dendritech (the company that produced the PAMAM dendrimer, 5 generations with an ethylenediamine core) MS results for a specific lot that was used by our team (please see Fig. S1†). The provided spectra indicate that the "naked" PAMAM has a major peak approximately at 26 kDa.

Finally, the UV spectra of both dendrimers, the "naked" and HSA-28D, clearly show a significant difference (Fig. S2†) in the intensity of absorption in the UV range. HSA-28 has two aromatic rings (phenylalanine and tyrosine), which are responsible

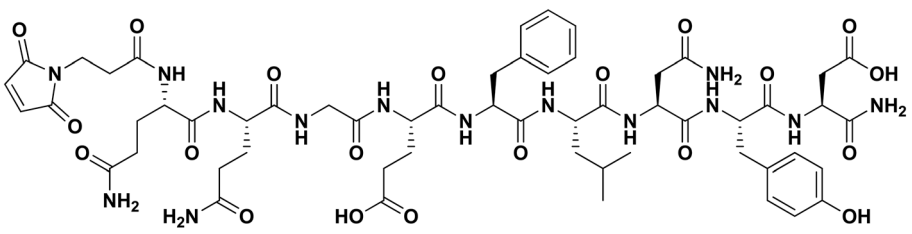

Mal-Gln-Gln-Gly-Glu-Phe-Leu-Asn-Tyr-Asp-NH_2

Scheme 1 Chemical structure of modified HSA-28 peptide.

Published on 13 December 2018. Downloaded by Bar Ilan University on 2/21/2019 4:40:40 AM.

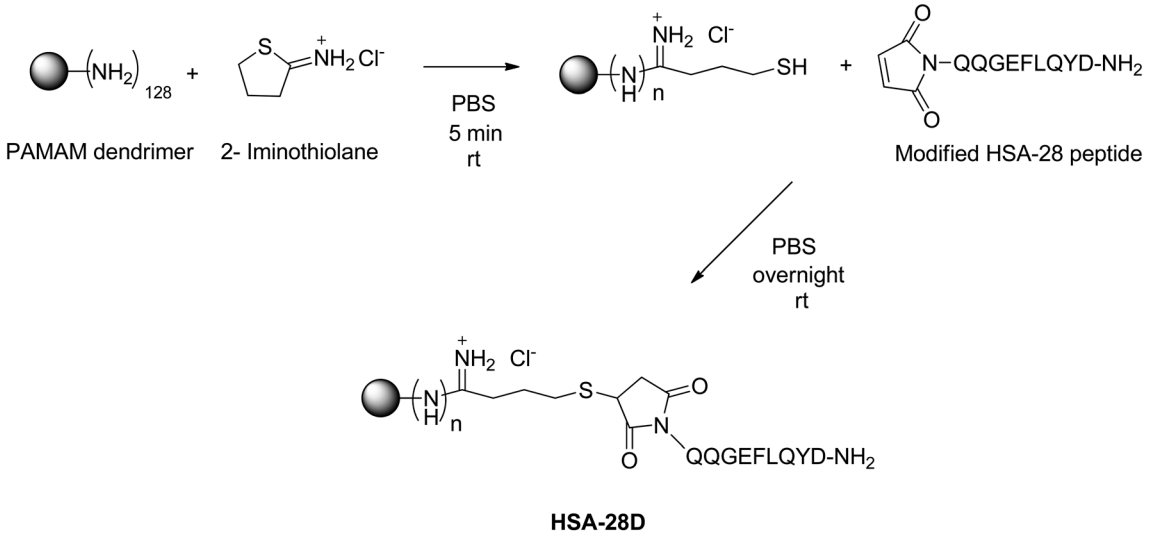

Scheme 2 General procedure for one-step preparation of HSA-28D.

for the absorption in the aromatic wavelength range. Obviously, the "naked" dendrimer does not have aromatic rings; hence, the absorption level in the UV range is very low compared with HSA-28D. Based on the results obtained from all these analytical techniques, the coupling of the peptide to the "naked" dendrimer should be considered as validated.

In vitro evaluation of HSA-28D biological activity

The possible effect of HSA-28D on the rate of cell proliferation was investigated using the INS-1E cell line. Fig. 1B shows that HSA-28D enhanced the rate of cell proliferation (around 40%) compared with untreated cells. The highest stimulatory effect on the proliferation rate was obtained after 72 h of incubation with HSA-28D (the concentration of the conjugated HSA-28D with PAMAM HSA-28 was 3 μg ml^{-1}). Interestingly, the non-coated PAMAM dendrimer exhibited a highly toxic effect toward the cells (data not shown).

The next goal was to determine the possible HSA-28D cell protective effect *in vitro*. To this end, two apoptosis-inducing systems were used: ER and oxidative stress. Both types of stress are involved in diabetes-related β-cell death.[59,60] To mimic ER stress *in vitro*, thapsigargin (Tg) was used.[61] The toxin dramatically elevates the intracellular levels of calcium and depletes ER calcium stores, thereby inducing ER stress. A glucose oxidase (GO)/glucose system was used as an inducer of oxidative stress.[62] We preferred to use this more controllable system to generate H_2O_2 than to directly add it to the medium at a high dose. The system continuously produces constant concentrations of H_2O_2. GO catalyzes the transfer of two oxygen electrons to H_2O_2, using reducing equivalents from the oxidation of glucose to glycolic acid. Glucose is present in the medium at a high concentration (to mimic the hyperglycemic conditions *in vivo*). Hence, the ROS generation never runs out because of the accessibility of the substrate to the enzymatic reaction.

Cells were incubated with HSA-28D and then exposed to Tg or GO. Fig. 1C shows that the compound has excellent cytoprotective characteristics by assisting cells in overcoming both types of stress conditions.

HSA-28D's effect on C-peptide, glucagon, and the PDX levels was investigated afterward. Determining the accumulation of C-peptide in β-cells is a common method for indirectly evaluating insulin production.[63,64] This small peptide links the two chains of insulin and assists in hormone maturation. Direct measurement of insulin *in vitro* can be problematic because, in addition to INS-1E-produced insulin, even the smallest amount of insulin from the growth medium masks the actual results. In contrast, C-peptide in different species is different, and C-peptide in FCS does not cross-react with the C-peptide from rat INS-1E cells. The ratio between C-peptide and insulin levels is 1 : 1 in secretory granules and both are secreted simultaneously.[65] INS-1E cells were treated with HSA-28D. Slides were obtained as described in "Methods" and the plasma membrane and nuclei were denoted by red and blue, respectively. Thereafter, slides were exposed to a primary antibody against C-peptide (green) and were evaluated by confocal microscopy. Cells treated with HSA-28P expressed surprisingly more C-peptide (approximately 6-fold) compared with untreated cells. (Fig. 1D). We normalized the intensity of the C-peptide level by the intensity of the membrane signal. Peptide alone and naked PAMAM did not have any effect on C-peptide accumulation (data not shown).

It is a known phenomenon that an increased proliferation rate of β-cell lines, such as INS-1E, leads to reduced differentiation levels.[66] Such a transformation might be manifested by abnormally elevated levels that are not related to β-cell hormones, for example, the production and secretion of the insulin antagonist, glucagon.[67] The basal levels of glucagon, which is still produced and secreted by INS-1E, might rise because of losing the phenotype; this is characterized by high

 This journal is © The Royal Society of Chemistry 2019

Published on 13 December 2018. Downloaded by Bar Ilan University on 2/21/2019 4:40:40 AM.

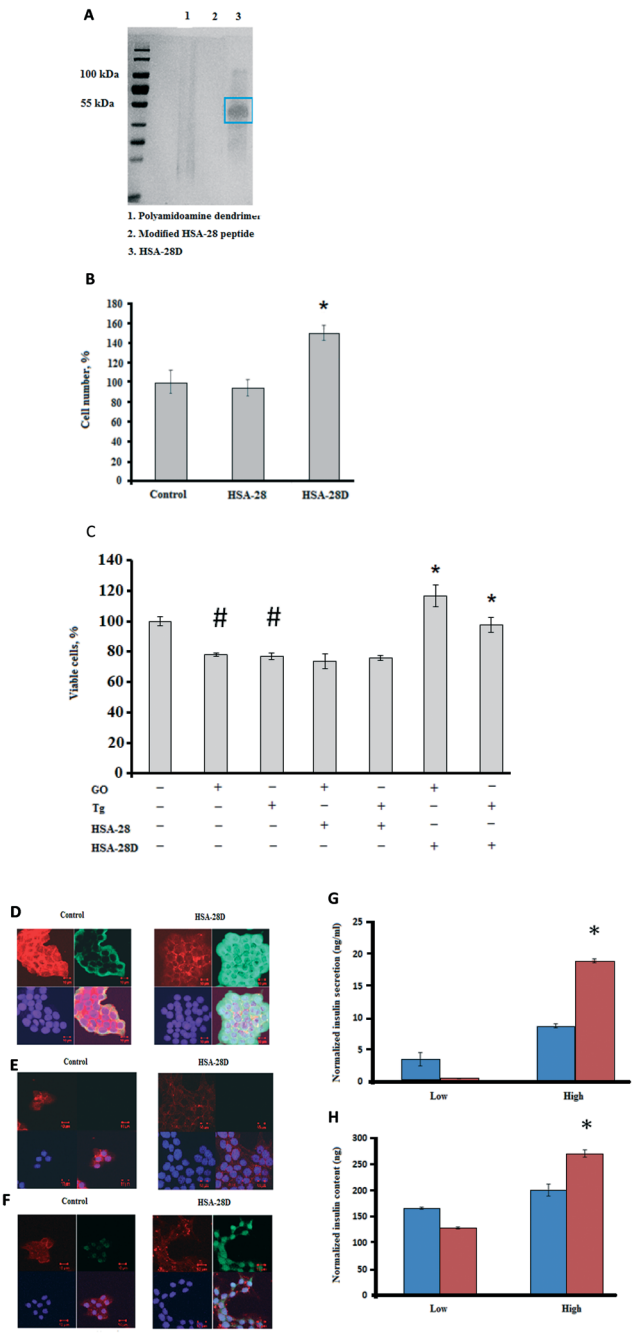

Fig. 1 (A) 6% SDS PAGE of HSA-28D. Samples (purified HSA-28D and loading buffer, 40 μl both) were boiled for 5 min, loaded to SDS PAGE, and run against TTS buffer. Bands were visualized using silver stain. (B) The effect of HSA-28D on the proliferation rate of INS-1E cells. INS-1E cells were seeded in 24-well plates and incubated for 72 h with the medium supplemented with HSA-28D ([HSA-28]-3 μg ml^{-1}). Thereafter, the cells were detached by trypsin, stained using trypan blue, and counted. The results are presented as a percentage compared to non-treated cells. *$p \leq 0.05$, $n = 6$. MEAN ± SE. (C) The effect of HSA-28D on cell viability under oxidative and ER stress conditions. INS-1E cells were incubated for 72 h with medium supplemented with HSA-28D ([HSA-28]-3 μg ml^{-1}). After incubation, 50 mU ml^{-1} glucose oxidase (GO) was added for an additional 1.15 h and 0.113 μg ml^{-1} thapsigargin (Tg) was added for an additional 24 hours. Upon completion of both experiments, a standard MTT assay was performed. The cell viability of both experiments is presented as a percentage compared to non-treated cells. *,#$p < 0.05$, $n = 3$. MEAN ± SE. (D) The effect of HSA-28D on C-peptide intracellular levels. Experiments were conducted on INS-1E cells that were seeded on coverslips in 6-well plates. INS-1E cells were incubated for 72 h with HSA-28D ([HSA-28]-3 μg ml^{-1}). Cells were fixed with formaldehyde, permeabilized, and exposed to anti-C-peptide or anti-glucagon (E) or anti-Pdx1 (F) antibodies, followed by secondary antibody (green). Thereafter, the cell membranes were exposed to Alexa Fluor 633 Phalloidin (red) and the nuclei were stained with DAPI (blue). Fluorescent signals were visualized with a confocal-Zeiss microscope. The experiment was run several times using the triplicate method, $n = 6$. Representative pictures are shown. The effect of HSA-28D on GSIS (G) and insulin content (H) under low and high glucose concentrations. The INS-1E cells (blue columns) were grown in 24-well plates and treated with HSA-28D ([HSA-28]-3 μg ml^{-1}) (red columns). After 72 h, the GSIS was evaluated in the presence of 3.3 mM (low) or 16.7 mM (high) glucose. H. Measurement of insulin content. The ELISA assay was performed for INS-1E lysates. *$p < 0.05$, $n = 3$. MEAN ± SE.

Published on 13 December 2018. Downloaded by Bar Ilan University on 2/21/2019 4:40:40 AM.

levels of differentiated β-cells.[68] Thus, the extent of intracellular accumulation of glucagon was investigated in INS-1E cells; as shown in Fig. 1E, HSA-28D did not lead to glucagon accumulation.

To further investigate the biological activity of HSA-28D, the possible effect of the compound on Pdx1 (pancreatic and duodenal homeobox 1) production was tested. Pdx1 is a transcription factor needed for pancreatic development and β-cell maturation.[69] Type 2 diabetes is characterized by the presence of a subpopulation of Pdx1-deficient β-cells.[70] The data presented in Fig. 1F clearly show that HSA-28D significantly elevated the basal level of the transcription factor (around 12 times).

Finally, the effect of HSA-28D on glucose-stimulated insulin secretion (GSIS) and insulin content in INS-1E cells was evaluated. HSA-28D significantly (around 2-fold) enhanced GSIS in comparison with non-treated cells (Fig. 1G). The total insulin content was also profoundly elevated upon treatment with HSA-28D in INS-1E cells, which were maintained at high glucose concentrations (Fig. 1H).

Pharmacophore-based design and synthesis of HSA-28 peptide mimetics

Peptides are one of the most abundant biomolecules in the physiology of any organism. However, the pharmacological use of peptides is very restricted because of their substantial problematic pharmacokinetic and pharmacodynamic properties, such as rapid proteolytic degradation, non-specific biological activity due to binding to "off target" macromolecules, low oral and even systemic bioavailability, the intense rate of elimination in the liver, and finally, also the high possibility of activating the immune system. To circumvent these challenging issues, several modern pharmacological approaches are in use: smart oral pharmaceutical formulations, slow release techniques, conjugates with organic molecules (usually polymers) that are targeted to specific tissues, peptides and peptidomimetics.[71–73] Peptidomimetics are small organic compounds that can mimic the peptide arrangement (pharmacophores) by replacing peptide functional groups and amide bonds by very similar structural domains and moieties. The 3D structures of peptides are closely reconstructed by peptidomimetics with the ability to interact and affect the biological targets. In contrast, the pharmacological and pharmacokinetic disadvantages of peptides are not present, due to changes in the covalent structures of these molecules.

Usually, computer modeling is used for designing a set of peptidomimetics, based on the structure of a known biologically active peptide. However, mimicking the structure of a long peptide such as HSA-28 (9 amino acids) was very

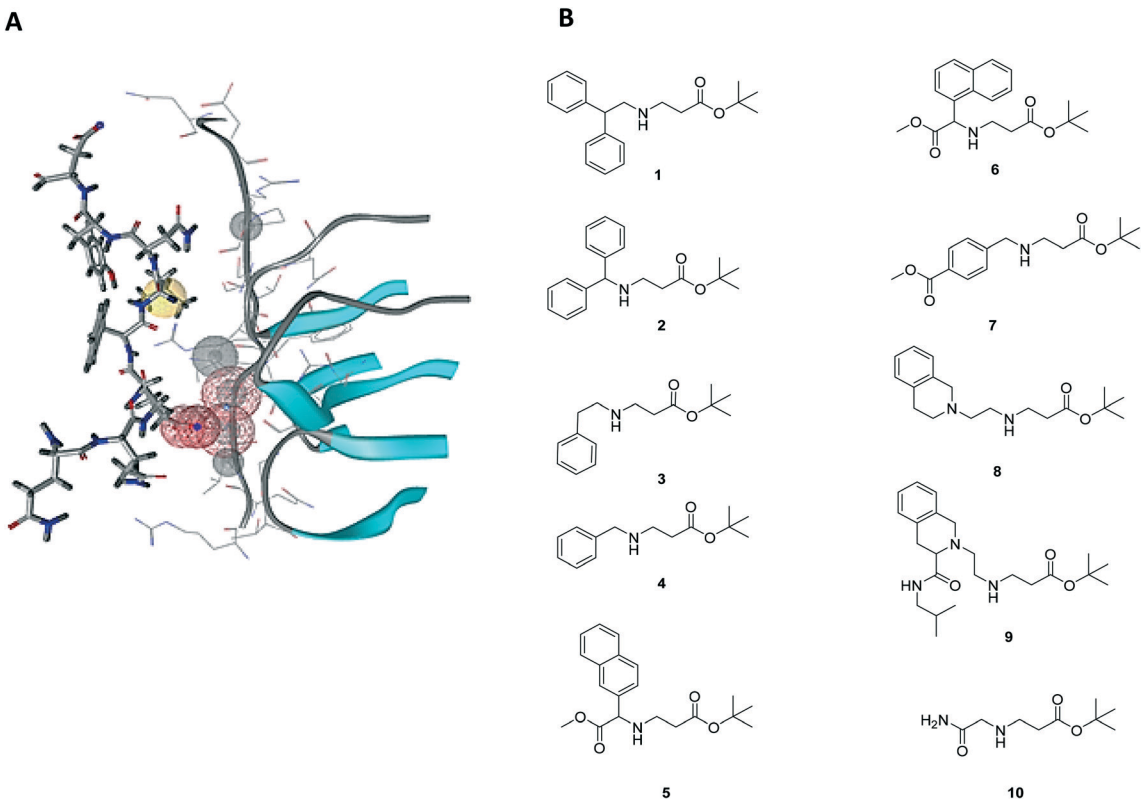

Fig. 2 (A). Pharmacophore design. Structure-based pharmacophore model generated with LigandScout from the structure of HSA-28 and NX-1. Pharmacophore features are color-coded: red represents negative charge features, yellow represents the hydrophobic feature, and gray represents excluded volumes. Excluded volumes are points in space occupied by protein atoms, which represent steric hindrances in the binding site. Such points cannot be occupied by ligand atoms. (B). The structures of the synthesized HSA-28 mimetics.

 This journal is © The Royal Society of Chemistry 2019

Published on 13 December 2018. Downloaded by Bar Ilan University on 2/21/2019 4:40:40 AM.

challenging. Thus, only side chains critical for the binding of glutamic, phenylalanine, and leucine amino acids were mimicked, as shown in Fig. 2A. The pharmacophore model was created, based on the structure of the complex between HSA-28 and NX-1 using LigandScout 4.0 software.[74]

Ten compounds (Fig. 2B) that fitted the pharmacophore model were synthesized: *tert*-butyl 3-((2,2-diphenylethyl)-amino)propanoate (**1**); *tert*-butyl 3-(benzhydrylamino)-propanoate (**2**); *tert*-butyl 3-(phenethylamino)propanoate (**3**); *tert*-butyl 3-(benzylamino)propanoate (**4**); *tert*-butyl 3-((2-methoxy-1-(naphthalen-2-yl)-2-oxoethyl)amino)propanoate (**5**); *tert*-butyl 3-((2-methoxy-1-(naphthalen-1-yl)-2-oxoethyl)amino)-propanoate (**6**); methyl 4-(((3-(*tert*-butoxy)-3-oxopropyl)amino)-methyl)benzoate (**7**); *tert*-butyl 3-((2-(3,4-dihydroisoquinolin-2(1*H*)-yl)ethyl)amino)propanoate (**8**); *tert*-butyl 3-((2-(3-(isobutylcarbamoyl)-3,4-dihydroisoquinolin-2(1*H*)-yl)ethyl)-amino)propanoate (**9**, novel compound); and *tert*-butyl 3-((2-amino-2-oxoethyl)amino)propanoate (**10**).

All compounds were obtained by a reaction between commercially available or synthesized in-house aromatic amines and *tert*-butyl acrylate (all synthetic procedures and analytical characterization studies are described in detail in the ESI†). All the synthesized final compounds were coupled with 3-maleimidopropionic acid and treated with TFA to remove the *tert*-butyl group. The obtained molecules were used for further conjugation to PAMAM NPs. The percentage of NPs used for covering was evaluated similarly to HSA-28D (the results are presented in the ESI,† Fig. S3).

The possible effect of all INS-1E cells being coated by peptidomimetic dendrimers was tested according to their proliferation rate. However, none of the compounds significantly affected the rate of cell proliferation (Fig. S4†).

Discussion

PAMAM dendrimers bring a unique possibility to create tree-like homogenous structures around one central core. The presence of free primary amine groups on the PAMAM surface allows a large spectrum of conjugational reactions. Regarding the attachment of biogenic peptides, it was shown that non-direct conjugation of a peptide to PAMAM *via* a PEG linker or in combination with an additional short linker is the most useful approach.[75–79] Different linkers besides PEG were also used for the biogenic peptide conjugation to PAMAM.[80–84] In addition, direct covering of PAMAM dendrimers by peptide was also reported.[85] However, to our knowledge we are the first to show the successful binding of a peptide to PAMAM using the 2-iminothiolane/malonic anhydride system. Indeed, A. Harada reported the conjugation of PAMAM *via* a 2-iminothiolane linker to polylysine; however, the S–S bond was used for coupling by the authors and not the peptide-3-(alkylthio)pyrrolidine-2,5-dione moiety, as we used.[86] To prove that HSA-28 conjugates with the PAMAM dendrimers to a sufficient extent, we applied a non-traditional method for the conjugation chemistry technique: SDS-PAGE. Based on the positions of the molecular weight markers, the average size (50 kDa) and the covering efficiency (around 16%) of the modified PAMAM dendrimers were identified (Fig. 1A).

It was shown that adult pancreatic β-cells still have a high ability to proliferate *in vivo* and that this self-duplication process is still important together with the generation of new β-cells from stem cells.[87,88] The observed ability of HSA-28D to increase the rate of INS-1E cell proliferation (see Fig. 1B) may be very important; further work is necessary to determine if the proliferative effect seen here with the INS-1 β-cell line would be seen also with primary β-cells. Prior results, however, demonstrate that NL-2 strongly influences the β-cell number *in vivo*.[29] Interestingly, cells treated with the compound were almost 50% more proliferative.

The most important observation here was related to the fact that HSA-28D was able to protect INS-1E cells against oxidative and ER stress, as shown in Fig. 1C. The β-cells are very sensitive towards oxidative stress because of their relatively weak molecular antioxidative defense system.[89] One of the major pathophysiological causes of diabetes is oxidative stress.[90] Lack of effective antioxidant protection triggers β-cell dysfunction in the early stage of diabetes followed by cell apoptosis in the progressive stages of the disease.[91] The combination of a low replication rate of the β-cells and the absence of a sufficient antioxidative response leads to cell death during diabetes.[92] Classical antioxidant therapy was tested in many clinical antidiabetic trials.[93] Unfortunately, direct antioxidative stress protection of β-cells and maintenance of β-cell mass were never achieved.[94] In addition to its own direct toxicity, oxidative stress causes total cellular dysfunction, which appears as cytosolic, mitochondrial, peroxisomal, or endoplasmic reticulum stress.[94] The latter plays a crucial role in diabetic β-cell apoptosis.[95] In general, ER stress is caused by a disproportion between the rate of proper protein folding and misfolding.[96] Misfolded proteins are unable to undergo degradation in proteasome or lysosome and accumulate in the ER lumen. In order to restore ER functionality, cells activate an emergency chain of actions termed unfolded protein response (UPR). There is substantial evidence for the presence of ER stress in diabetic β-cells.[97] Chronic ER stress leads to apoptosis.[98] ER stress was also targeted as a possible site for a pharmacological intervention to protect β-cells under diabetic conditions.[99,100] The use of chemical and more specific pharmaceutical chaperones, prevention of eIF2B inhibition, calcium leak blockers, stimulators of ER folding capacities, and other groups of compounds was proposed.[95] However, using this approach, substantial progress in β-cell protection has not yet been achieved.

HSA-28D displayed a significant protective effect in β-cells that were maintained under both main apoptotic triggers (ER and oxidative stress). In light of the failure of conventional anti-oxidative stress and anti-ER stress therapeutic approaches for diabetes, such a dual effect might play a very important role in the future development of NL-2 mimetic-based β-cells for protective therapy.

Published on 13 December 2018. Downloaded by Bar Ilan University on 2/21/2019 4:40:40 AM.

It is known that non-covered PAMAM dendrimers (especially cationic ones) are extremely toxic for cells.[101–104] According to our experience, INS-1E cells died at a 34.6 μM concentration of a "naked" PAMAM dendrimer. This observation was in agreement with recently published articles about the toxicity of PAMAMs.[105,106] In addition, it is also known that in general, high concentrations of positively charged polyamines can destroy and damage the plasma membrane and kill animal cells.[107,108] However, by covering PAMAM nanoparticles with peptides (even at 16%), positively charged amines can be eliminated by creating a neutral amide bond. Thus, covered PAMAM (even partially) was not toxic to the cells in biologically active concentrations.

The test compound dramatically increased C-peptide (insulin) accumulation in INS-1E cells (Fig. 1D). Cells incubated with HSA-28D in the presence of 22.5 mM glucose for 72 h enhanced the intracellular insulin content almost 6-fold. These data support our hypothesis that mimicking NL-2/NX interaction between β-cells leads to high levels of maturation of those cells and not only to increased proliferation. The stability of the β-cell phenotype after treatment with HSA-28D was proved by the absence of glucagon in the cytosol (Fig. 1E). Moreover, the high maturation of the treated cells was also indicated by the increased intracellular levels of PDX1. PDX1 is a master transcription factor that tightly regulates pancreatic development, the β-cell proliferation, and most importantly, sufficient structural and functional maturation of β-cells.[109] Normal expression of PDX1 in β-cells blocks glucagon expression and selectively promotes the expression of β-cell-specific genes.[110] It is important to mention that T2DM is characterized not only by apoptosis of the β-cells but also by dematuration of β-cells and their transdifferentiation to different types of cells (usually to α-cells). PDX1-deficient β-cells are found in progressive T2DM.[111] Apoptosis, low rates of proliferation, and transdifferentiation lead to a constant decline in β-cell mass during the progression of T2D and these result in a constant failure to generate enough new β-cells. It was very encouraging that under HSA-28D treatment, PDX1 levels in INS-1E were significantly elevated (Fig. 1F), suggesting that the increased insulin accumulation in treated cells is attributed to increased maturation.

The most important test for the functionality of the observed effects of the test compound on INS-1E was GSIS. As shown in Fig. 1G, three days of administration of HSA-28D led to a significant augmentation of the rate of insulin secretion under physiological conditions (medium glucose level 13 mM). Interestingly, INS-1E cells treated with the test compound slightly decreased basal insulin secretion. These results underscored two very important issues related to the HSA-28D mode of action: the insulin secretion occurred only as a physiological response to elevated glucose levels and not by some non-specific leaking of insulin from damaged plasma membranes. Second, large quantities of insulin that accumulated during three days of exposing the cell to the test compound were able to be secreted physiologically. Measured by ELISA, the cell insulin content was also markedly high in the treated HSA-28D cells (Fig. 1H) and these results were correlated with the results that we obtained by fluorescence microscopy (Fig. 1G). However, the difference was considerably lower than that obtained fluorescently (6-fold in the fluorescence method *versus* 2.1-fold in the colorimetric method), which might be explained by the higher sensitivity of fluorescence detection. Alternatively, the maturation of insulin granules in HSA-28D treated cells might also explain the difference.

To overcome possible low bioavailability and other pharmacokinetically related disadvantages, our next step in the project was to try to develop peptidomimetics based on the HSA-28 structure. Such molecules (conjugated to PAMAM), on the one hand, might mimic the 3D structure of the native peptide, but on the other hand, non-peptide bonds and non-natural amino acid moieties should create more biologically stable molecules with identical or even upgraded activity. Based on the *in silico* pharmacophore model, feasible structures for the organic synthetic compounds were created and fitted to the model. After evaluation of the *in silico* binding score, the first ten molecules were synthesized. We tried to mimic the three most important interactions/natural amino acid moieties in HSA-28, such as the branched lipophilic moiety of leucine, the charged carboxylic acid of glutamic acid, and finally, the phenyl moiety of phenylalanine.

Compound **9** is a novel peptidomimetic obtained in 7-step synthesis with a linear yield of 24%. Such a molecule might be used for general glutamic, phenylalanine, and leucine amino acid mimetics in the development of mimetics absolutely non-relevant to NL-2 peptidomimetics.

A proliferation assay was used for evaluating molecules covered by ten peptidomimetic PAMAMs. Unfortunately, none of the synthesized molecules had a positive effect on the INS-1E proliferation rate (Fig. S4†). This disappointing result can be explained by the fact that the peptide conformations chosen for mimicking the peptide interactions *in silico* might not be reproducible by peptidomimetics when they are conjugated to PAMAM. In addition, it is also possible that for sufficient mimicking of NL-2 interactions with NXs, an entire scaffold of nine amino acids is essential. In this case, the synthesis of a nine amino acid peptidomimetic sequence can be very challenging.

In summary, the ability of the functionalized NPs reported here to prevent β-cells's substantial apoptosis, an increase in their mass, maturation, and most importantly, their ability to secrete insulin in a glucose-dependent manner might be used for developing novel β-cell protective therapeutic agents and β-cell transplantation supporters, especially considering that a PAMAM-based core for such NPs is biocompatible.

Conflicts of interest

The authors declare no conflict of interest.

 This journal is © The Royal Society of Chemistry 2019

Published on 13 December 2018. Downloaded by Bar Ilan University on 2/21/2019 4:40:40 AM.

Acknowledgements

This study was supported by a Bar-Ilan University new faculty grant, a D-cure (Diabetes Care in Israel) Young Investigator Award, and a NOFAR program (Israel Ministry of Industry) for A. G. The Israel Science Foundation (application number 117/2014) provided a grant for A. G. and J.-P. L. In addition, S. K. is thankful for the support of her work by the Wolf Foundation. S. D. C. was supported by NIH/NIDDK grant R01DK080971. G. C. is partially supported by the Israel Ministry of Science and Technology. This work was also funded by the 7th Framework RTD European Project (FP7-530 NMP-2010-LARGE-4 area) – Large Collaborative Projects – Project 531 SaveMe (grant agreement no. 263307) for J.-P. L. and finally, by The Bar-University Rector's Grant for Interdisciplinary Research (2017) for A. G., J.-P. L. and H. S. We would like to thank Steve Manch for the English editing of the manuscript.

References

1 A. Weisman, G. S. Fazli, A. Johns and G. L. Booth, Evolving Trends in the Epidemiology, Risk Factors, and Prevention of Type 2 Diabetes: A Review, *Can. J. Cardiol.*, 2018, **34**, 552–564.

2 W. D. Strain, S. V. Hope, A. Green, P. Kar, J. Valabhji and A. J. Sinclair, Type 2 diabetes mellitus in older people: a brief statement of key principles of modern day management including the assessment of frailty. A national collaborative stakeholder initiative, *Diabet. Med.*, 2018, **35**, 838–845.

3 J. R. Petrie, T. J. Guzik and R. M. Touyz, Diabetes, Hypertension, and Cardiovascular Disease: Clinical Insights and Vascular Mechanisms, *Can. J. Cardiol.*, 2018, **34**, 575–584.

4 H. Mulder and C. Ling, Mitochondrial dysfunction in pancreatic beta-cells in Type 2 diabetes, *Mol. Cell. Endocrinol.*, 2009, **297**, 34–40.

5 E. U. Alejandro, B. Gregg, M. Blandino-Rosano, C. Cras-Meneur and E. Bernal-Mizrachi, Natural history of beta-cell adaptation and failure in type 2 diabetes, *Mol. Aspects Med.*, 2015, **42**, 19–41.

6 C. Chen, C. M. Cohrs, J. Stertmann, R. Bozsak and S. Speier, Human beta cell mass and function in diabetes: Recent advances in knowledge and technologies to understand disease pathogenesis, *Mol. Metab.*, 2017, **6**, 943–957.

7 I. Song, C. Muller, J. Louw and L. Bouwens, Regulating the beta cell mass as a strategy for type-2 diabetes treatment, *Curr. Drug Targets*, 2015, **16**, 516–524.

8 R. Scharfmann, M. Didiesheim, P. Richards, V. Chandra, M. Oshima and O. Albagli, Mass production of functional human pancreatic beta-cells: why and how?, *Diabetes, Obes. Metab.*, 2016, **18**(Suppl 1), 128–136.

9 S. Pellegrini, E. Cantarelli, V. Sordi, R. Nano and L. Piemonti, The state of the art of islet transplantation and cell therapy in type 1 diabetes, *Acta Diabetol.*, 2016, **53**, 683–691.

10 Y. Evron, C. K. Colton, B. Ludwig, G. C. Weir, B. Zimermann, S. Maimon, T. Neufeld, N. Shalev, T. Goldman, A. Leon, K. Yavriyants, N. Shabtay, T. Rozenshtein, D. Azarov, A. R. DiIenno, A. Steffen, P. de Vos, S. R. Bornstein, U. Barkai and A. Rotem, Long-term viability and function of transplanted islets macroencapsulated at high density are achieved by enhanced oxygen supply, *Sci. Rep.*, 2018, **8**, 6508.

11 P. Mondal, A. Prasad and K. Girdhar, Interventions to improve beta-cell mass and function, *Ann. Endocrinol.*, 2017, **78**, 469–477.

12 S. Tritschler, F. J. Theis, H. Lickert and A. Bottcher, Systematic single-cell analysis provides new insights into heterogeneity and plasticity of the pancreas, *Mol. Metab.*, 2017, **6**, 974–990.

13 J. Shirakawa, D. F. De Jesus and R. N. Kulkarni, Exploring inter-organ crosstalk to uncover mechanisms that regulate beta-cell function and mass, *Eur. J. Clin. Nutr.*, 2017, **71**, 896–903.

14 M. Okamoto, T. Ishizaki and T. Kimura, Protective effect of hydrogen sulfide on pancreatic beta-cells, *Nitric Oxide*, 2015, **46**, 32–36.

15 J. S. Danobeitia, P. J. Chlebeck, I. Shokolenko, X. Ma, G. Wilson and L. A. Fernandez, Novel Fusion Protein Targeting Mitochondrial DNA Improves Pancreatic Islet Functional Potency and Islet Transplantation Outcomes, *Cell Transplant.*, 2017, **26**, 1742–1754.

16 J. J. Yin, Y. B. Li, Y. Wang, G. D. Liu, J. Wang, X. O. Zhu and S. H. Pan, The role of autophagy in endoplasmic reticulum stress-induced pancreatic beta cell death, *Autophagy*, 2012, **8**, 158–164.

17 S. Z. Safi, R. Qvist, G. Ong, H. Karimian, M. Imran and I. Shah, Stimulation of beta-adrenergic receptors plays a protective role via increased expression of RAF-1 and PDX-1 in hyperglycemic rat pancreatic islet (RIN-m5F) cells, *Arch. Med. Sci.*, 2017, **13**, 470–480.

18 D. A. Cunha, M. Cito, P. O. Carlsson, J. M. Vanderwinden, J. D. Molkentin, M. Bugliani, P. Marchetti, D. L. Eizirik and M. Cnop, Thrombospondin 1 protects pancreatic beta-cells from lipotoxicity via the PERK-NRF2 pathway, *Cell Death Differ.*, 2016, **23**, 1995–2006.

19 J. Chen, S. T. Hui, F. M. Couto, I. N. Mungrue, D. B. Davis, A. D. Attie, A. J. Lusis, R. A. Davis and A. Shalev, Thioredoxin-interacting protein deficiency induces Akt/Bcl-xL signaling and pancreatic beta-cell mass and protects against diabetes, *FASEB J.*, 2008, **22**, 3581–3594.

20 A. Kaminitz, S. Ash and N. Askenasy, Neutralization Versus Reinforcement of Proinflammatory Cytokines to Arrest Autoimmunity in Type 1 Diabetes, *Clin. Rev. Allergy Immunol.*, 2017, **52**, 460–472.

21 C. S. Hampe, Protective role of anti-idiotypic antibodies in autoimmunity–lessons for type 1 diabetes, *Autoimmunity*, 2012, **45**, 320–331.

22 A. Fierabracci, Peptide immunotherapies in Type 1 diabetes: lessons from animal models, *Curr. Med. Chem.*, 2011, **18**, 577–586.

Published on 13 December 2018. Downloaded by Bar Ilan University on 2/21/2019 4:40:40 AM.

23 N. S. Wilcox, J. Rui, M. Hebrok and K. C. Herold, Life and death of beta cells in Type 1 diabetes: A comprehensive review, *J. Autoimmun.*, 2016, **71**, 51–58.
24 C. M. Hull, M. Peakman and T. I. M. Tree, Regulatory T cell dysfunction in type 1 diabetes: what's broken and how can we fix it?, *Diabetologia*, 2017, **60**, 1839–1850.
25 A. Itoh and W. M. Ridgway, Targeting innate immunity to downmodulate adaptive immunity and reverse type 1 diabetes, *ImmunoTargets Ther.*, 2017, **6**, 31–38.
26 J. Ludvigsson, Therapies to Preserve beta-Cell Function in Type 1 Diabetes, *Drugs*, 2016, **76**, 169–185.
27 A. Munder, L. L. Israel, S. Kahremany, R. Ben-Shabat-Binyamini, C. Zhang, M. Kolitz-Domb, O. Viskind, A. Levine, H. Senderowitz, S. Chessler, J. P. Lellouche and A. Gruzman, Mimicking Neuroligin-2 Functions in beta-Cells by Functionalized Nanoparticles as a Novel Approach for Antidiabetic Therapy, *ACS Appl. Mater. Interfaces*, 2017, **9**, 1189–1206.
28 C. Zhang, A. T. Suckow and S. D. Chessler, Coculture analysis of extracellular protein interactions affecting insulin secretion by pancreatic beta cells, *J. Visualized Exp.*, 2013, e50365.
29 C. Zhang, A. T. Suckow and S. D. Chessler, Altered pancreatic islet function and morphology in mice lacking the Beta-cell surface protein neuroligin-2, *PLoS One*, 2013, **8**, e65711.
30 A. T. Suckow, C. Zhang, S. Egodage, D. Comoletti, P. Taylor, M. T. Miller, I. R. Sweet and S. D. Chessler, Transcellular neuroligin-2 interactions enhance insulin secretion and are integral to pancreatic beta cell function, *J. Biol. Chem.*, 2012, **287**, 19816–19826.
31 A. T. Suckow, D. Comoletti, M. A. Waldrop, M. Mosedale, S. Egodage, P. Taylor and S. D. Chessler, Expression of neurexin, neuroligin, and their cytoplasmic binding partners in the pancreatic beta-cells and the involvement of neuroligin in insulin secretion, *Endocrinology*, 2008, **149**, 6006–6017.
32 R. A. R. Villacis, J. S. Filho, B. Pina, R. B. Azevedo, A. Pic-Taylor, J. F. Mazzeu and C. K. Grisolia, Integrated assessment of toxic effects of maghemite (gamma-Fe2O3) nanoparticles in zebrafish, *Aquat. Toxicol.*, 2017, **191**, 219–225.
33 G. Qualhato, T. L. Rocha, E. C. de Oliveira Lima, E. S. DM, J. R. Cardoso, C. Koppe Grisolia and S. M. T. de Saboia-Morais, Genotoxic and mutagenic assessment of iron oxide (maghemite-gamma-Fe2O3) nanoparticle in the guppy Poecilia reticulata, *Chemosphere*, 2017, **183**, 305–314.
34 V. Dhakshinamoorthy, V. Manickam and E. Perumal, Neurobehavioural Toxicity of Iron Oxide Nanoparticles in Mice, *Neurotoxic. Res.*, 2017, **32**, 187–203.
35 D. Astruc, C. Deraedt, R. Djeda, C. Ornelas, X. Liu, A. Rapakousiou, J. Ruiz, Y. Wang and Q. Wang, Dentromers, a Family of Super Dendrimers with Specific Properties and Applications, *Molecules*, 2018, **23**, 966.
36 J. Li, H. Liang, J. Liu and Z. Wang, Poly (amidoamine) (PAMAM) dendrimer mediated delivery of drug and pDNA/siRNA for cancer therapy, *Int. J. Pharm.*, 2018, **546**, 215–225.
37 Y. Kim, E. J. Park and D. H. Na, Recent progress in dendrimer-based nanomedicine development, *Arch. Pharmacal Res.*, 2018, **41**, 571–582.
38 B. Gomes, M. T. Augusto, M. R. Felicio, A. Hollmann, O. L. Franco, S. Goncalves and N. C. Santos, Designing improved active peptides for therapeutic approaches against infectious diseases, *Biotechnol. Adv.*, 2018, **36**, 415–429.
39 R. Nuti, N. S. Goud, A. P. Saraswati, R. Alvala and M. Alvala, Antimicrobial Peptides: A Promising Therapeutic Strategy in Tackling Antimicrobial Resistance, *Curr. Med. Chem.*, 2017, **24**, 4303–4314.
40 G. Trapani, C. Satriano and D. La Mendola, Peptides and their Metal Complexes in Neurodegenerative Diseases: from Structural Studies to Nanomedicine Prospects, *Curr. Med. Chem.*, 2018, **25**, 715–747.
41 M. Wang, K. P. Rakesh, J. Leng, W. Y. Fang, L. Ravindar, D. Channe Gowda and H. L. Qin, Amino acids/peptides conjugated heterocycles: A tool for the recent development of novel therapeutic agents, *Bioorg. Chem.*, 2018, **76**, 113–129.
42 H. Bruzzoni-Giovanelli, V. Alezra, N. Wolff, C. Z. Dong, P. Tuffery and A. Rebollo, Interfering peptides targeting protein-protein interactions: the next generation of drugs?, *Drug Discovery Today*, 2018, **23**, 272–285.
43 W. Shen and T. Matsui, Current knowledge of intestinal absorption of bioactive peptides, *Food Funct.*, 2017, **8**, 4306–4314.
44 J. Richard, Challenges in oral peptide delivery: lessons learnt from the clinic and future prospects, *Ther. Delivery*, 2017, **8**, 663–684.
45 T. Mavromoustakos, S. Durdagi, C. Koukoulitsa, M. Simcic, M. G. Papadopoulos, M. Hodoscek and S. G. Grdadolnik, Strategies in the rational drug design, *Curr. Med. Chem.*, 2011, **18**, 2517–2530.
46 A. Mizuno, K. Matsui and S. Shuto, From Peptides to Peptidomimetics: A Strategy Based on the Structural Features of Cyclopropane, *Chemistry*, 2017, **23**, 14394–14409.
47 N. Qvit, S. J. S. Rubin, T. J. Urban, D. Mochly-Rosen and E. R. Gross, Peptidomimetic therapeutics: scientific approaches and opportunities, *Drug Discovery Today*, 2017, **22**, 454–462.
48 M. A. Blaskovich, Unusual Amino Acids in Medicinal Chemistry, *J. Med. Chem.*, 2016, **59**, 10807–10836.
49 P. Zer-Aviv, M. Shubely, Y. Moskovits, O. Viskind, A. Albeck, D. Vertommen, S. Ruthstein, M. Shokhen and A. Gruzman, A new oxopiperazin-based peptidomimetic molecule inhibits prostatic acid phosphatase secretion and induces prostate cancer cells apoptosis, *ChemistrySelect*, 2016, **1**, 4658–4667.
50 R. Behrendt, P. White and J. Offer, Advances in Fmoc solid-phase peptide synthesis, *J. Pept. Sci.*, 2016, **22**, 4–27.
51 L. Pasternak, E. Meltzer-Mats, G. Babai-Shani, G. Cohen, O. Viskind, J. Eckel, E. Cerasi, S. Sasson and A. Gruzman, Benzothiazole derivatives augment glucose uptake in skeletal muscle cells and stimulate insulin secretion from

 This journal is © The Royal Society of Chemistry 2019

Published on 13 December 2018. Downloaded by Bar Ilan University on 2/21/2019 4:40:40 AM.

pancreatic beta-cells via AMPK activation, *Chem. Commun.*, 2014, **50**, 11222–11225.

52 R. Shapira, S. Rudnick, B. Daniel, O. Viskind, V. Aisha, M. Richman, K. R. Ayasolla, A. Perelman, J. H. Chill, A. Gruzman and S. Rahimipour, Multifunctional cyclic D,L-alpha-peptide architectures stimulate non-insulin dependent glucose uptake in skeletal muscle cells and protect them against oxidative stress, *J. Med. Chem.*, 2013, **56**, 6709–6718.

53 V. Rosengren, H. Johansson, J. Lehtio, L. Fransson, A. Sjoholm and H. Ortsater, Thapsigargin down-regulates protein levels of GRP78/BiP in INS-1E cells, *J. Cell. Biochem.*, 2012, **113**, 1635–1644.

54 G. Cohen, O. Shamni, Y. Avrahami, O. Cohen, E. C. Broner, N. Filippov-Levy, C. Chatgilialoglu, C. Ferreri, N. Kaiser and S. Sasson, Beta cell response to nutrient overload involves phospholipid remodelling and lipid peroxidation, *Diabetologia*, 2015, **58**, 1333–1343.

55 M. Muchtaridi, H. N. Syahidah, A. Subarnas, M. Yusuf, S. D. Bryant and T. Langer, Molecular Docking and 3D-Pharmacophore Modeling to Study the Interactions of Chalcone Derivatives with Estrogen Receptor Alpha, *Pharmaceuticals*, 2017, **10**, 81.

56 P. Ingallinella, D. Fattori, S. Altamura, C. Steinkuhler, U. Koch, D. Cicero, R. Bazzo, R. Cortese, E. Bianchi and A. Pessi, Prime site binding inhibitors of a serine protease: NS3/4A of hepatitis C virus, *Biochemistry*, 2002, **41**, 5483–5492.

57 P. Ruzza, A. Calderan, A. Donella-Deana, B. Biondi, L. Cesaro, A. Osler, S. Elardo, A. Guiotto, L. A. Pinna and G. Borin, Conformational constraints of tyrosine in protein tyrosine kinase substrates: Information about preferred bioactive side-chain orientation, *Biopolymers*, 2003, **71**, 478–488.

58 P. Chaumet-Riffaud, I. Martinez-Duncker, A. L. Marty, C. Richard, A. Prigent, F. Moati, L. Sarda-Mantel, D. Scherman, M. Bessodes and N. Mignet, Synthesis and application of lactosylated, 99mTc chelating albumin for measurement of liver function, *Bioconjugate Chem.*, 2010, **21**, 589–596.

59 J. Wang, X. Yang and J. Zhang, Bridges between mitochondrial oxidative stress, ER stress and mTOR signaling in pancreatic beta cells, *Cell. Signalling*, 2016, **28**, 1099–1104.

60 S. Z. Hasnain, J. B. Prins and M. A. McGuckin, Oxidative and endoplasmic reticulum stress in beta-cell dysfunction in diabetes, *J. Mol. Endocrinol.*, 2016, **56**, R33–R54.

61 I. Yoshida, A. Monji, K. Tashiro, K. Nakamura, R. Inoue and S. Kanba, Depletion of intracellular Ca2+ store itself may be a major factor in thapsigargin-induced ER stress and apoptosis in PC12 cells, *Neurochem. Int.*, 2006, **48**, 696–702.

62 S. Kahremany, I. Babaev, P. Hasin, T. Tamir, T. Ben-Zur, G. Cohen, Z. Jiang, S. Weintraub, D. Offen, S. Rahimipour, B. Major, H. Senderowitz and A. Gruzman, Computer-aided design and synthesis of (1-(4-((3,4-dihydroxybenzylidene)-amino)phenyl)-5-oxopyrrolidine-3-carboxylic acid) as a novel Nrf2 enhancer, *ChemPlusChem*, 2018, **83**, 320–333.

63 A. Castell-Auvi, L. Cedo, V. Pallares, M. Blay, M. Pinent and A. Ardevol, Grape seed procyanidins improve beta-cell functionality under lipotoxic conditions due to their lipid-lowering effect, *J. Nutr. Biochem.*, 2013, **24**, 948–953.

64 M. Fukaya, C. A. Brorsson, K. Meyerovich, L. Catrysse, D. Delaroche, E. C. Vanzela, F. Ortis, R. Beyaert, L. B. Nielsen, M. L. Andersen, H. B. Mortensen, F. Pociot, G. van Loo, J. Storling and A. K. Cardozo, A20 Inhibits beta-Cell Apoptosis by Multiple Mechanisms and Predicts Residual beta-Cell Function in Type 1 Diabetes, *Mol. Endocrinol.*, 2016, **30**, 48–61.

65 A. H. Rubenstein, D. F. Steiner, D. L. Horwitz, M. E. Mako, M. B. Block, J. I. Starr, H. Kuzuya and F. Melani, Clinical significance of circulating proinsulin and C-peptide, *Recent Prog. Horm. Res.*, 1976, **33**, 435–475.

66 M. Vincent, Y. Guz, M. Rozenberg, G. Webb, M. Furuta, D. Steiner and G. Teitelman, Abrogation of protein convertase 2 activity results in delayed islet cell differentiation and maturation, increased alpha-cell proliferation, and islet neogenesis, *Endocrinology*, 2003, **144**, 4061–4069.

67 J. C. Schisler, P. B. Jensen, D. G. Taylor, T. C. Becker, F. K. Knop, S. Takekawa, M. German, G. C. Weir, D. Lu, R. G. Mirmira and C. B. Newgard, The Nkx6.1 homeodomain transcription factor suppresses glucagon expression and regulates glucose-stimulated insulin secretion in islet beta cells, *Proc. Natl. Acad. Sci. U. S. A.*, 2005, **102**, 7297–7302.

68 L. C. Bollheimer, C. E. Wrede, F. Rockmann, I. Ottinger, J. Scholmerich and R. Buettner, Glucagon production of the rat insulinoma cell line INS-1-A quantitative comparison with primary rat pancreatic islets, *Biochem. Biophys. Res. Commun.*, 2005, **330**, 327–332.

69 K. A. D'Amour, A. G. Bang, S. Eliazer, O. G. Kelly, A. D. Agulnick, N. G. Smart, M. A. Moorman, E. Kroon, M. K. Carpenter and E. E. Baetge, Production of pancreatic hormone-expressing endocrine cells from human embryonic stem cells, *Nat. Biotechnol.*, 2006, **24**, 1392–1401.

70 K. Fujimoto and K. S. Polonsky, Pdx1 and other factors that regulate pancreatic beta-cell survival, *Diabetes, Obes. Metab.*, 2009, **11**(Suppl 4), 30–37.

71 A. M. Wagner, M. P. Gran and N. A. Peppas, Designing the new generation of intelligent biocompatible carriers for protein and peptide delivery, *Acta Pharm. Sin. B*, 2018, **8**, 147–164.

72 P. Batista, P. M. Castro, A. R. Madureira, B. Sarmento and M. Pintado, Recent insights in the use of nanocarriers for the oral delivery of bioactive proteins and peptides, *Peptides*, 2018, **101**, 112–123.

73 S. H. Wang and J. Yu, Structure-based design for binding peptides in anti-cancer therapy, *Biomaterials*, 2018, **156**, 1–15.

74 G. Wolber and T. Langer, LigandScout: 3-D pharmacophores derived from protein-bound ligands and their use as virtual screening filters, *J. Chem. Inf. Model.*, 2005, **45**, 160–169.

Published on 13 December 2018. Downloaded by Bar Ilan University on 2/21/2019 4:40:40 AM.

75 S. V. K. Rompicharla, P. Kumari, B. Ghosh and S. Biswas, Octa-arginine modified poly(amidoamine) dendrimers for improved delivery and cytotoxic effect of paclitaxel in cancer, *Artif. Cells, Nanomed., Biotechnol.*, 2018, 1–13.

76 P. Ma, J. Chen, X. Bi, Z. Li, X. Gao, H. Li, H. Zhu, Y. Huang, J. Qi and Y. Zhang, Overcoming Multidrug Resistance through the GLUT1-Mediated and Enzyme-Triggered Mitochondrial Targeting Conjugate with Redox-Sensitive Paclitaxel Release, *ACS Appl. Mater. Interfaces*, 2018, **10**, 12351–12363.

77 Q. Hu, Q. Chen, X. Yan, B. Ding, D. Chen and L. Cheng, Chondrocyte affinity peptide modified PAMAM conjugate as a nanoplatform for targeting and retention in cartilage, *Nanomedicine*, 2018, **13**, 749–767.

78 Y. Wang, L. Wang, G. Chen and S. Gong, Carboplatin-Complexed and cRGD-Conjugated Unimolecular Nanoparticles for Targeted Ovarian Cancer Therapy, *Macromol. Biosci.*, 2017, **17**, 1600292.

79 Z. Chen, F. Lian, X. Wang, Y. Chen and N. Tang, Arginine-glycine-aspartic acid-polyethylene glycol-polyamidoamine dendrimer conjugate improves liver-cell aggregation and function in 3-D spheroid culture, *Int. J. Nanomed.*, 2016, **11**, 4247–4259.

80 E. Orocio-Rodriguez, G. Ferro-Flores, C. L. Santos-Cuevas, M. Ramirez Fde, B. E. Ocampo-Garcia, E. Azorin-Vega and F. M. Sanchez-Garcia, Two Novel Nanosized Radiolabeled Analogues of Somatostatin for Neuroendocrine Tumor Imaging, *J. Nanosci. Nanotechnol.*, 2015, **15**, 4159–4169.

81 A. Ghai, B. Singh, P. Panwar Hazari, M. K. Schultz, A. Parmar, P. Kumar, S. Sharma, D. Dhawan and A. Kumar Mishra, Radiolabeling optimization and characterization of (68)Ga labeled DOTA-polyamido-amine dendrimer conjugate - Animal biodistribution and PET imaging results, *Appl. Radiat. Isot.*, 2015, **105**, 40–46.

82 S. P. Kambhampati, M. K. Mishra, P. Mastorakos, Y. Oh, G. A. Lutty and R. M. Kannan, Intracellular delivery of dendrimer triamcinolone acetonide conjugates into microglial and human retinal pigment epithelial cells, *Eur. J. Pharm. Biopharm.*, 2015, **95**, 239–249.

83 A. Satsangi, S. S. Roy, R. K. Satsangi, R. K. Vadlamudi and J. L. Ong, Design of a paclitaxel prodrug conjugate for active targeting of an enzyme upregulated in breast cancer cells, *Mol. Pharmaceutics*, 2014, **11**, 1906–1918.

84 L. Y. Jiang, B. Lv and Y. Luo, The effects of an RGD-PAMAM dendrimer conjugate in 3D spheroid culture on cell proliferation, expression and aggregation, *Biomaterials*, 2013, **34**, 2665–2673.

85 S. L. Mekuria and H. C. Tsai, Preparation of self-assembled core-shell nano structure of conjugated generation 4.5 poly (amidoamine) dendrimer and monoclonal Anti-IL-6 antibody as bioimaging probe, *Colloids Surf., B*, 2015, **135**, 253–260.

86 A. Harada, R. Matsuki, S. Ichimura, E. Yuba and K. Kono, Intracellular environment-responsive stabilization of polymer vesicles formed from head-tail type polycations composed of a polyamidoamine dendron and poly(L-lysine), *Molecules*, 2013, **18**, 12168–12179.

87 X. Xu, J. D'Hoker, G. Stange, S. Bonne, N. De Leu, X. Xiao, M. Van de Casteele, G. Mellitzer, Z. Ling, D. Pipeleers, L. Bouwens, R. Scharfmann, G. Gradwohl and H. Heimberg, Beta cells can be generated from endogenous progenitors in injured adult mouse pancreas, *Cell*, 2008, **132**, 197–207.

88 Y. Dor, J. Brown, O. I. Martinez and D. A. Melton, Adult pancreatic beta-cells are formed by self-duplication rather than stem-cell differentiation, *Nature*, 2004, **429**, 41–46.

89 S. Lenzen, Oxidative stress: the vulnerable beta-cell, *Biochem. Soc. Trans.*, 2008, **36**, 343–347.

90 C. M. O. Volpe, P. H. Villar-Delfino, P. M. F. Dos Anjos and J. A. Nogueira-Machado, Cellular death, reactive oxygen species (ROS) and diabetic complications, *Cell Death Dis.*, 2018, **9**, 119.

91 M. Tiedge, S. Lortz, J. Drinkgern and S. Lenzen, Relation between antioxidant enzyme gene expression and antioxidative defense status of insulin-producing cells, *Diabetes*, 1997, **46**, 1733–1742.

92 W. Wang, C. Liu, M. Jimenez-Gonzalez, W. J. Song and M. A. Hussain, The undoing and redoing of the diabetic beta-cell, *J. Diabetes Complications*, 2017, **31**, 912–917.

93 R. Rahimi, S. Nikfar, B. Larijani and M. Abdollahi, A review on the role of antioxidants in the management of diabetes and its complications, *Biomed. Pharmacother.*, 2005, **59**, 365–373.

94 S. Lenzen, Chemistry and biology of reactive species with special reference to the antioxidative defence status in pancreatic beta-cells, *Biochim. Biophys. Acta*, 2017, **1861**, 1929–1942.

95 M. Cnop, S. Toivonen, M. Igoillo-Esteve and P. Salpea, Endoplasmic reticulum stress and eIF2alpha phosphorylation: The Achilles heel of pancreatic beta cells, *Mol. Metab.*, 2017, **6**, 1024–1039.

96 R. Y. Hampton, ER stress response: getting the UPR hand on misfolded proteins, *Curr. Biol.*, 2000, **10**, R518–521.

97 D. L. Eizirik, A. K. Cardozo and M. Cnop, The role for endoplasmic reticulum stress in diabetes mellitus, *Endocr. Rev.*, 2008, **29**, 42–61.

98 D. T. Rutkowski and R. J. Kaufman, A trip to the ER: coping with stress, *Trends Cell Biol.*, 2004, **14**, 20–28.

99 A. L. Clark and F. Urano, Endoplasmic reticulum stress in beta cells and autoimmune diabetes, *Curr. Opin. Immunol.*, 2016, **43**, 60–66.

100 C. Evans-Molina, M. Hatanaka and R. G. Mirmira, Lost in translation: endoplasmic reticulum stress and the decline of beta-cell health in diabetes mellitus, *Diabetes, Obes. Metab.*, 2013, **15**(Suppl 3), 159–169.

101 R. Duncan and L. Izzo, Dendrimer biocompatibility and toxicity, *Adv. Drug Delivery Rev.*, 2005, **57**, 2215–2237.

102 F. P. Seib, A. T. Jones and R. Duncan, Comparison of the endocytic properties of linear and branched PEIs, and cationic PAMAM dendrimers in B16f10 melanoma cells, *J. Controlled Release*, 2007, **117**, 291–300.

103 W. Lesniak, A. U. Bielinska, K. Sun, K. W. Janczak, X. Shi, J. R. Baker, Jr and L. P. Balogh, Silver/dendrimer nanocomposites as biomarkers: fabrication, characterization,

 This journal is © The Royal Society of Chemistry 2019

Published on 13 December 2018. Downloaded by Bar Ilan University on 2/21/2019 4:40:40 AM.

in vitro toxicity, and intracellular detection, *Nano Lett.*, 2005, **5**, 2123–2130.

104 J. F. Kukowska-Latallo, K. A. Candido, Z. Cao, S. S. Nigavekar, I. J. Majoros, T. P. Thomas, L. P. Balogh, M. K. Khan and J. R. Baker, Jr, Nanoparticle targeting of anticancer drug improves therapeutic response in animal model of human epithelial cancer, *Cancer Res.*, 2005, **65**, 5317–5324.

105 L. Albertazzi, L. Gherardini, M. Brondi, S. Sulis Sato, A. Bifone, T. Pizzorusso, G. M. Ratto and G. Bardi, In vivo distribution and toxicity of PAMAM dendrimers in the central nervous system depend on their surface chemistry, *Mol. Pharmaceutics*, 2013, **10**, 249–260.

106 P. C. Naha and H. J. Byrne, Generation of intracellular reactive oxygen species and genotoxicity effect to exposure of nanosized polyamidoamine (PAMAM) dendrimers in PLHC-1 cells in vitro, *Aquat. Toxicol.*, 2013, **132–133**, 61–72.

107 C. S. Hayes, K. DeFeo-Mattox, P. M. Woster and S. K. Gilmour, Elevated ornithine decarboxylase activity promotes skin tumorigenesis by stimulating the recruitment of bulge stem cells but not via toxic polyamine catabolic metabolites, *Amino Acids*, 2014, **46**, 543–552.

108 M. Li, Q. Li, Y. H. Zhang, Z. Y. Tian, H. X. Ma, J. Zhao, S. Q. Xie and C. J. Wang, Antitumor effects and preliminary systemic toxicity of ANISpm in vivo and in vitro, *Anti-Cancer Drugs*, 2013, **24**, 32–42.

109 M. L. Stitzel, I. Kycia, R. Kursawe and D. Ucar, Transcriptional Regulation of the Pancreatic Islet: Implications for Islet Function, *Curr. Diabetes Rep.*, 2015, **15**, 66.

110 W. Wang, S. Jin and K. Ye, Development of Islet Organoids from H9 Human Embryonic Stem Cells in Biomimetic 3D Scaffolds, *Stem Cells Dev.*, 2017, **26**, 394–404.

111 J. Sun, L. Q. Mao, K. S. Polonsky and D. C. Ren, Pancreatic beta-Cell Death due to Pdx-1 Deficiency Requires Multi-BH Domain Protein Bax but Not Bak, *J. Biol. Chem.*, 2016, **291**, 13529–13534.

Electronic Supplementary Material (ESI) for MedChemComm.
This journal is © The Royal Society of Chemistry 2019

Supporting Information

Covered by Neuroligin-2 derived peptide polyamidoamine-based (PAMAM) dendrimers enhance pancreatic β-cells proliferation and functions

Anna Munder,[a] Yoni Moskovitz,[a] Aviv Meir,[a] Shirin Kahremany, [ab] Laura Levy,[a] Michal Kolitz-Domb,[a] Guy Cohen,[c] Efrat Shtriker,[a] Olga Viskind,[a] Jean-Paul Lellouche,[ad] Hanoch Senderowitz,[a] Steven D. Chessler,[e] Edward E. Korshin,[a] Sharon Ruthstein,[a] and Arie Gruzman*[a]

[a]Department of Chemistry, Faculty of Exact Sciences, Bar-Ilan University, Ramat-Gan, Israel.

[b]Department of Pharmacology, Cleveland Center for Membrane and Structural Biology, School of Medicine, Case Western Reserve University, Cleveland, OH, USA

[c]Skin Research Institute, Dead Sea and Arava Research Center, Masada, Israel

[d]Nanomaterials Research Center, Institute of Nanotechnology & Advanced Materials (BINA), Bar-Ilan University, Ramat-Gan, Israel

[e]Division of Endocrinology, Diabetes & Metabolism, Department of Medicine, University of California, Irvine, CA, USA

Table of contents

1. Materials

PAMAM dendrimer (ethylenediamine core, fifth generation), bovine serum albumin (BSA), glucose oxidase (GO), thapsigargin (Tg), protease inhibitor cocktail, radioimmunoprecipitation assay buffer (RIPA), rink amide resin, 2,2-diphenylethylamine, benzhydrylamine, phenethylamine, benzylamine, glycinamide hydrochloride, α-and β-naphataldehyde, 1,2,3,4–tetraisoquinoline, n-bromoethylphtalimide, potassium carbonate, potassium iodide, tert-butyl acrylate, isobutylamine, triethylamine, 2-iminothiolane, 3-maleimidopropionic acid were purchased from Sigma-Aldrich (Merk),(Rehovot, Israel). Fetal calf serum (FCS), phosphate buffered saline (PBS), L-glutamine, Trypan blue, Roswell Park Memorial Institute medium (RPMI-1640), and antibiotics were purchased from Biological Industries (Beth-Haemek, Israel). Formaldehyde (4% in PBS) was purchased from Bio-Lab (Jerusalem, Israel). Rink amide resin, DIEA, protected amino acids were obtained from Chem Impex (Wood Dale, IL, USA). *β*-Mercaptoethanol was purchased from Bio-Rad (Hercules, CA, USA). Alfa Aesar (Ward Hill, MA, USA) supplied t-isopropanol-silane. Alexa Fluor 633 Phalloidin was purchased from Life Technologies (Carlsbad, CA, USA). Anti-glucagon, anti-C-peptide and anti-Pdx1 antibodies were supplied by Abcam (Cambridge, MA, USA). Mercodia Insulin ELISA kit was purchased from Mercodia (Uppsala, Sweden). All organic solvents were purchased from Carlo Erba Reagents (Val De Reuil, France).

2. Characterization data of modified HSA-28 peptide

a. Mass spectroscopy analytical data

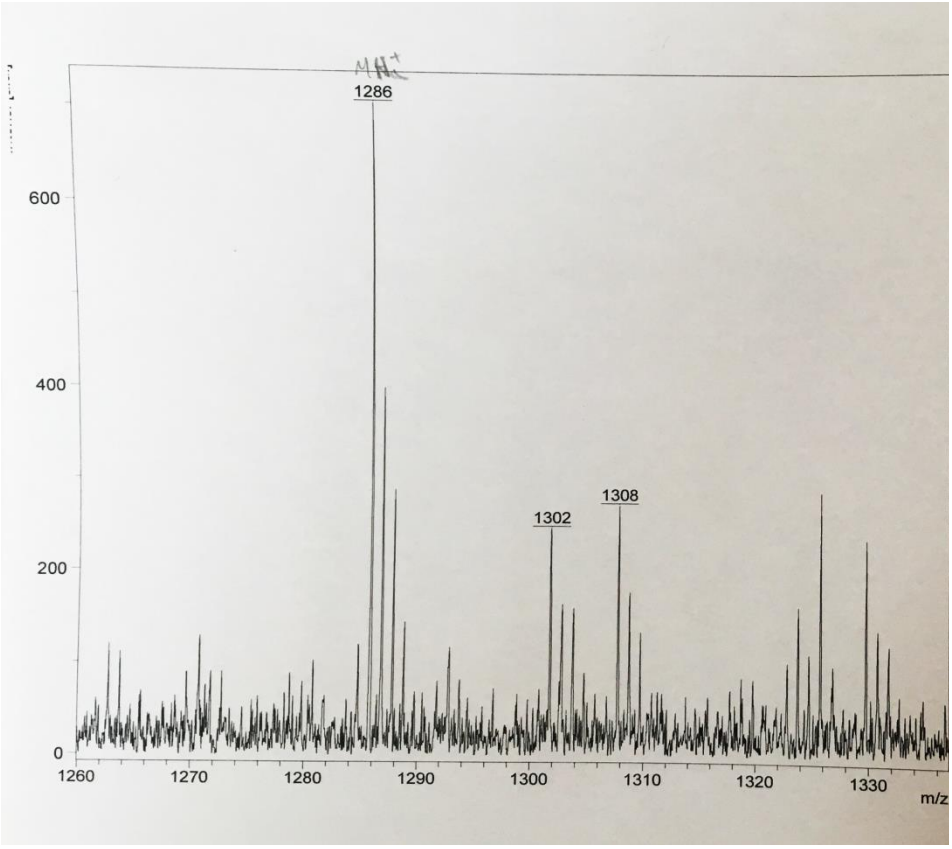

b. HPLC analytical data

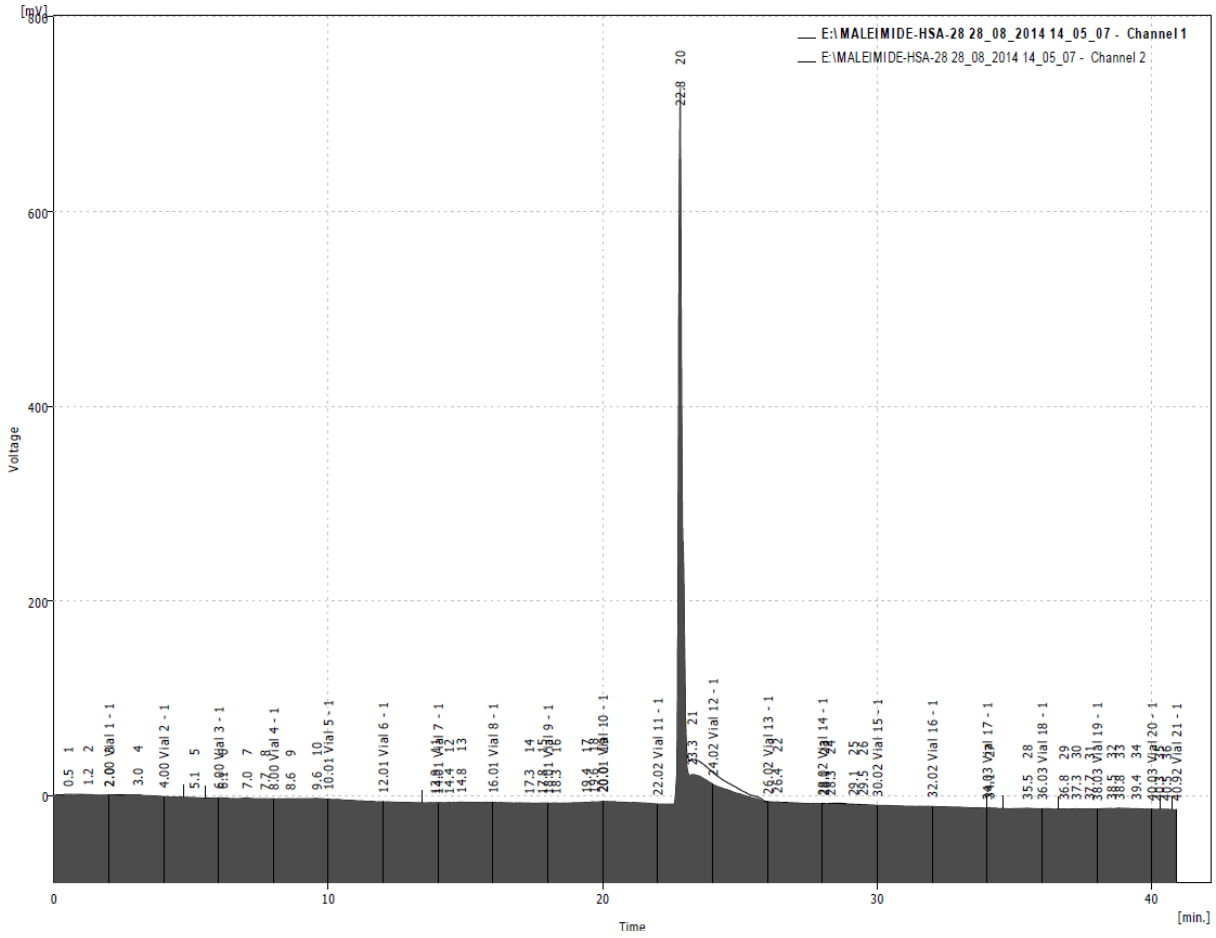

3. Synthetic procedures

General procedure for the synthesis of tert-butylaminopropanoates (**1-4**).

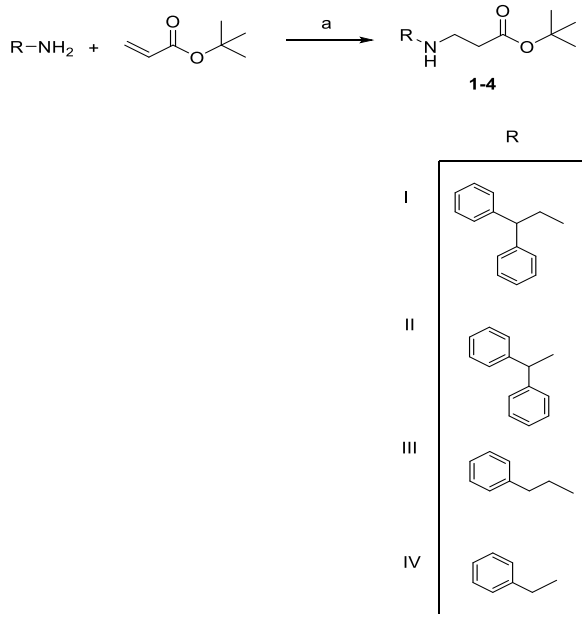

Scheme 1. *Synthesis of compounds **1-4***. Reagents and conditions. (a) EtOH, rt, overnight.

Tert-butyl acrylate (10 mmol) was added dropwise to the appropriate aromatic amines (**I**, 2,2-diphenylethylamine; **II**, benzhydrylamine; **III**, phenethylamine, **IV**, benzylamine, 10 mmol in EtOH, 5 ml). Stirring at rt was continued overnight. The reaction progress was followed by TLC (DCM/EtOAc 1:1, 1% TEA). After completion of the reaction, EtOH was evaporated under reduced pressure to yield colorless to yellow oil. The compounds were purified by column chromatography using the same conditions as in TLC monitoring.

General procedure for the synthesis tert-butyl 3-((2-methoxy-1-(naphthalen-1-yl)-2-oxoethyl)amino)propanoate (**5**) and tert-butyl 3-((2-methoxy-1-(naphthalen-2-yl)-2-oxoethyl)amino)propanoate (**6**)

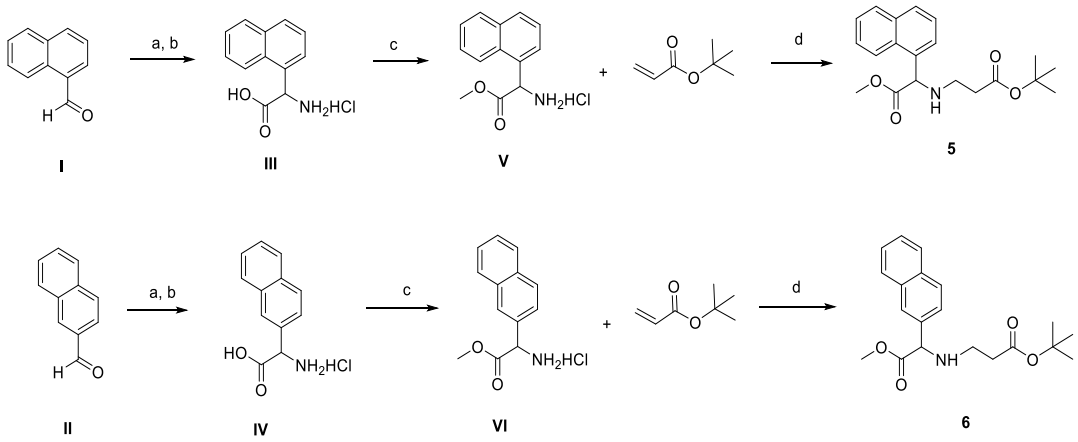

Scheme 2. *Synthesis of compounds **5, 6.*** Reagents and conditions. (a) KCN, NH_4Cl, NH_4OH (30%), rt, overnight. (b) HCl, reflux, 2h. (c) $SOCl_2$, MeOH, reflux, 6h. (d) TEA, MeOH, rt, 48h.

Potassium cyanide (28 mmol) and ammonium chloride (28 mmol) were dissolved in 100 ml of aqueous solution of ammonia (30%). The solution was cooled on ice bath to 5 ^{0}C. Commercially available α- or β-naphtaldehyde (**I** and **II**, respectively, 12 mmol) were then added in three portions with 5 min intervals. The obtained mixture was stirred overnight at rt. Then, the mixture was diluted with 100 ml of water and extracted twice with 100 ml of toluene. The toluene fraction was extracted twice with 60 ml 6N HCl. The aqueous acidic layer was refluxed for 2h, then cooled to 0 ^{0}C, affording white to cream crystals that were collected by suction filtration. α- Naphtylphenyl glycine hydrochloride (**III**) and β-naphtylphenyl glycine hydrochloride (**IV**), respectively, were taken to the next step without any purification. Next, α- naphtylphenyl glycine hydrochloride or β- naphtylphenyl glycine hydrochloride (**III**, **IV**, respectively, 10 mmol) was dissolved in thionyl chloride

(0.05 mol) and the solution was stirred for 1h at rt. After the indicated time, the solution was cooled on ice bath and 100 ml of MeOH and an additional amount of thionyl chloride (0.05 mol) was added. The obtained solution was refluxed for 6 h, cooled, and the solvent was evaporated under reduced pressure. The product was precipitated from a minimum amount of MeOH by the addition of diethyl ether. Methyl 2-amino-2-(naphthalen-1-yl)acetate (**V**) or methyl 2-amino-2-(naphthalen-2-yl)acetate (**VI**) were taken to the next step without any purification. Finally, compounds **V** or **VI** from the previous step (0.5 mmol) were dissolved in 25 ml of MeOH followed by the addition of an equivalent amount of TEA. Tert-butyl acrylate (0.5 mmol) was dissolved in 10 ml of MeOH and the mixture was added dropwise to solutions of compounds **V** or **VI**. The mixture was stirred at rt for 48h.The monitoring of the reaction was performed through TLC (hexane/EtOAc 6:4, 2% TEA). After the indicated time, the solvent was evaporated under reduced pressure and compounds were purified by column chromatography using hexane/EtOAc 6:4, 2% TEA as an eluent to obtain compounds **5** or **6**, respectively, as light brown oil.

General procedure for the synthesis methyl 4-(((3-(tert-butoxy)-3-oxopropyl)amino)methyl)benzoate (**7**)

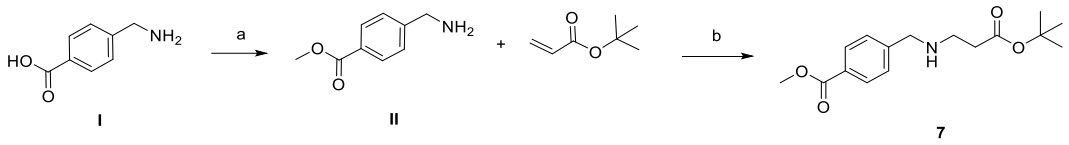

Scheme 3. *Synthesis of compound 7.* Reagents and conditions. (a) $SOCl_2$, MeOH, reflux, 6h. (b) TEA, MeOH, rt, overnight.

Commercially available 4-aminomethylbenzoate (**I**, 0.02 mol) was refluxed in MeOH (50 ml) for 6h in the presence of thionyl chloride (0.04 mol). After the indicated time, the mixture was cooled on the ice bath and the white precipitate was filtered, affording pure methyl 4-(aminomethyl)benzoate (**II**). In the next step, the obtained compound was reacted with tert-butyl acrylate by a method that was described above, yielding compound **7**. Monitoring of the reaction was performed using a mixture of hexane/EtOAc (6:4) in the presence of 1% TEA. The purification of 7 was performed by column chromatography using the same eluent.

General procedure for the synthesis tert-butyl 3-((2-(3,4-dihydroisoquinolin-2(1H)-yl)ethyl)amino)propanoate (**8**)

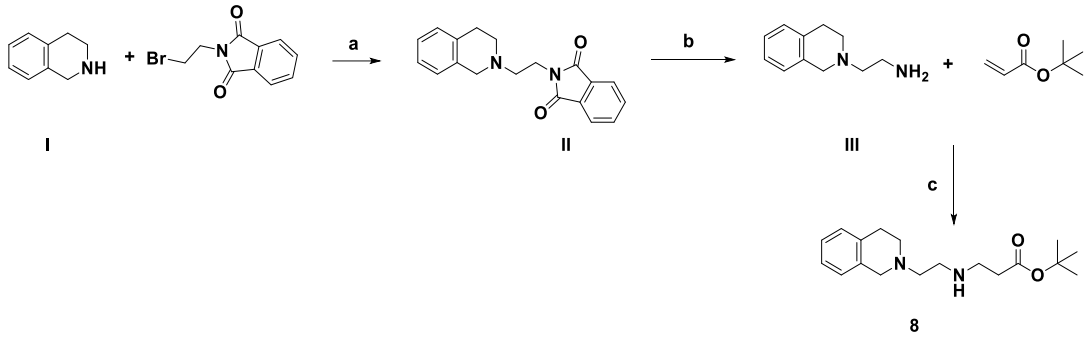

Scheme 4. *Synthesis of compound **8.*** Reagents and conditions. (a) K_2CO_3, KI, MeCN, reflux, 4h. (b) hydrazine hydrate, EtOH, reflux, 2h. (c) EtOH, rt, overnight

Commercially available 1,2,3,4-tetraisoquinoline (**I**) (10 mmol) was dissolved in MeCN and treated with n-bromoethylphtalimide (12.5 mmol), potassium carbonate (30 mmol), and potassium iodide (12.5 mmol). The mixture was refluxed for 4h. After the indicated time, the reaction solution was filtered and the filtrate was evaporated under reduced pressure. The residue was dissolved in EtOAc and the solution was acidified with 2N of HCl followed by extraction with water. The pH of the aqueous phase was adjusted to pH 12 with 4N NaOH and extracted with DCM. Evaporation of the organic solvent afforded 2-(2-(3,4-dihydroisoquinolin-2(1H)-yl)ethyl)isoindoline-1,3-dione (**II**), which was taken to the next step without any purification. In the next step, the latter compound was dissolved in 40 ml of EtOH and 19 mmol of hydrazine hydrate was added to the solution. The reaction was refluxed for 2h and cooled to rt. The precipitation was gravitationally filtered and the filtrate was concentrated under vacuum. The residue was dissolved in 40

ml EtOAc, filtered, and evaporated again, affording 2-(3,4-dihydroisoquinolin-2(1H)-yl)ethan-1-amine (**III**), which was taken to the next step without purification. Finally, **III** was reacted with tert-butyl acrylate by a method described before, affording compound **8**. The monitoring of the reaction and the purification by column chromatography were performed under the same conditions mentioned above.

General procedure for the synthesis tert-butyl 3-((2-(3-(isobutylcarbamoyl)-3,4-dihydroisoquinolin-2(1H)-yl) ethyl) amino) propanoate (**9**)

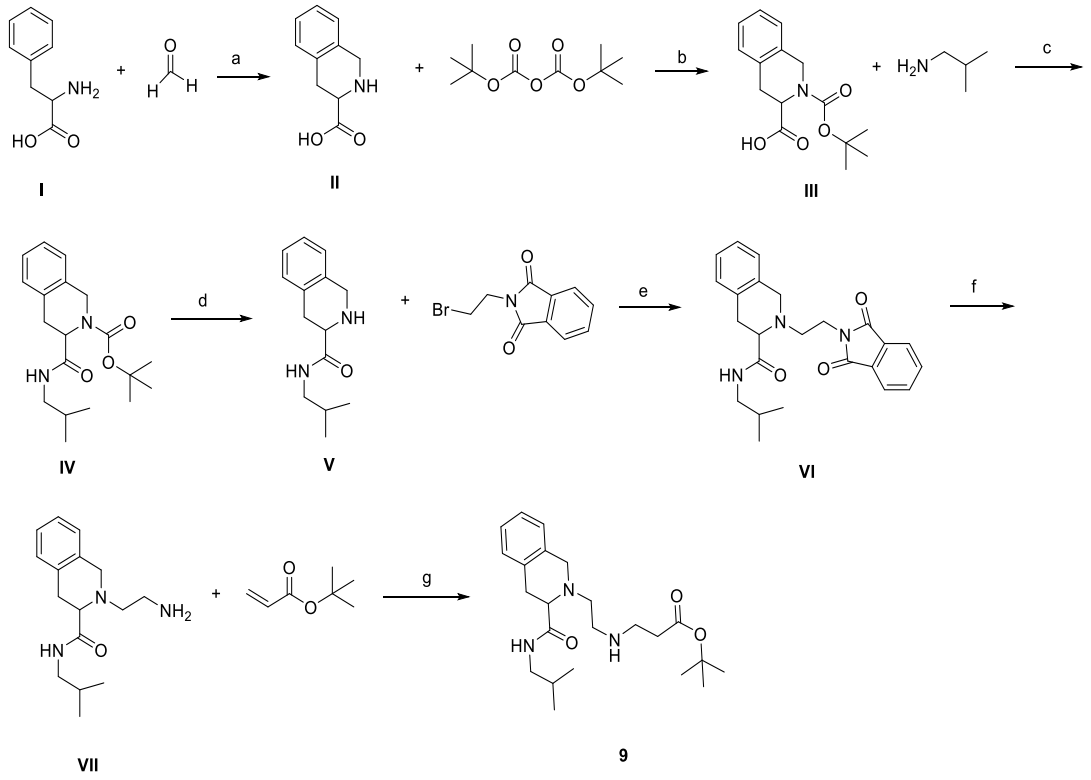

Scheme 5. *Synthesis of compound **9**.* Reagents and conditions. (a) 32% HCl, H_2SO_4, reflux, 48h. (b) NaOH, THF, H_2O, rt, 48h. (c) DCC, HOSu, TEA, DCM, rt, overnight. (d) DCM/TFA (1:1), rt, 1h. (e) K_2CO_3, KI, MeCN, reflux, overnight. (f) hydrazine hydrate, EtOH, reflux, 2h. (g) EtOH, rt, overnight.

Cyclization of commercially available L-phenylalanine (**I**) (0.015 mmol) was performed by reaction with an excess of paraformaldehyde (2 gr) in the presence of concentrated sulfuric for the corresponding 1, 2, 3, 4-tetrahydroisoquinoline-3-carboxylic acid (**II**). Briefly, the amino acid was dissolved in 32% hydrochloric acid (50 ml), followed by the

addition of 0.5 ml of sulfuric acid. The solution was refluxed for 48h, cooled, and filtered. The resulting solid was dissolved in a hot mixture of H2O/EtOH (1:1, 25 ml) and basified with ammonium hydroxide (30%) until pH 7.0. The obtained crystals were collected by filtration, washed with two portions of EtOH, affording **II**, which was taken to the next step without any purification.

In the next step, the secondary amine of **II** was protected by Boc protecting group to afford 2-(tert-butoxycarbonyl)-1,2,3,4-tetrahydroisoquinoline-3-carboxylic acid **III**. Briefly, 1, 2, 3, 4-tetrahydroisoquinoline-3-carboxylic acid (0.01 mol) and sodium hydroxide (0.015 mol) were dissolved in water and a solution of di-tert-butyl dicarbonate (0.016 mol) in THF (10 ml) was added dropwise. After having been stirred for 48h at rt, the solvent was evaporated, the residue was dissolved in EtOAc (25 ml), and washed with 5% $KHSO_4$ and brine. The organic solvent was dried over sodium sulphate, and evaporated, leading to 2-(tert-butoxycarbonyl)-1,2,3,4-tetrahydroisoquinoline-3-carboxylic acid (**III**).

In the next step, commercially available isobutylamine was coupled to a carboxylic moiety of **III** by DCC coupling reagent and HOSu to obtain tert-butyl 3-(isobutylcarbamoyl)-3,4-dihydroisoquinoline-2(1H)-carboxylate **IV**, followed by removal of Boc protecting group by TFA, leading to N-isobutyl-1,2,3,4-tetrahydroisoquinoline-3-carboxamide **V**. Isobutylamine (0.006 mol) was dissolved in DCM (50 ml). DCC (0.006 mol), HOSu (0.006 mol), and TEA (0.006 mol) were added to the solution followed by the addition of **III** (0.006 mol). After having been stirred overnight at rt, the mixture was cooled and filtered, and the filtrate was washed with 2% $KHSO_4$ and 5% $NaHCO_3$, dried over magnesium sulphate, filtered, and evaporated, affording IV tert-butyl 3-(isobutylcarbamoyl)-3,4-dihydroisoquinoline-2(1H)-carboxylate. The compound was

dissolved in a mixture of DCM/TFA 1:1 (20 ml) and the mixture was stirred for 1h, followed by evaporation of solvent, leading to 3-(isobutylcarbamoyl)-3,4-dihydroisoquinoline-2(1H)-carboxylate, **V**.

In the next step, a secondary amine of V was alkylated with bromoethylphtalimide (**VI**), followed by the removal of the phatlimide moiety by hydrazine hydrate (**VII**) and finally, 2-(2-aminoethyl)-N-isobutyl-1,2,3,4-tetrahydroisoquinoline-3-carboxamide (**VII**) was reacted with tert-butyl acrylate by the same method described before, affording **9**. The purification of 9 was performed through column chromatography using a mixture of hexane/EtOAc (8:2) as an eluent.

General procedure for the synthesis tert-butyl 3-((2-amino-2-oxoethyl)amino)propanoate (**10**)

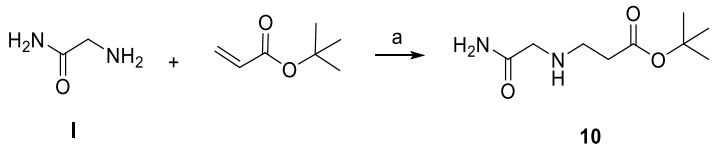

I 10

Scheme 6. *Synthesis of compound **10**.* Reagents and conditions. (a) EtOH, TEA, 40 ^{0}C, 48h**.**

Glycinamide hydrochloride (**I**, 10 mmol) and TEA (10 mmol) were added to 70 ml of EtOH. The mixture was heated to 40 ^{0}C and stirred until all solids were completely dissolved. Then, 10 mmol of tert-butyl acrylate was mixed with 5 ml of EtOH and the mixture was added dropwise to the solution of glycinamide. Stirring at 40 ^{0}C was continued for 48h. The reaction progress was followed by TLC (hexane/EtOAc 8:2, 1% TEA) and

visualized in the iodide atmosphere. After completion of the reaction, EtOH was evaporated under reduced pressure to yield a colorless syrup. Compound 10 was purified by column chromatography using the same conditions as those used in TLC monitoring.

Coupling of compounds (**1-10**) to 3-maleimidopropionic acid followed by removal of t-butoxyl protecting group

3-maleimidopropionic acid was conjugated to compounds **1-10** (as described before) followed by deprotection of the t-butoxyl protecting group by neat TFA. All compounds purified by HPLC (gradient water/MeCN from 100% of water in 80 min, flow = 2 ml/min, λ = 210, λ = 254 nm).

4. NMR spectra images

tert-butyl 3-((2,2-diphenylethyl)amino)propanoate (**1**)

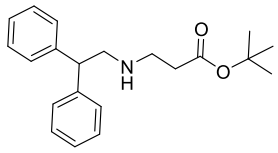

Yield 79%, pale yellow oil. ^{1}H NMR ($CDCl_3$, 400 MHz): δ 1.356 (s, 9H,), δ 2.362 (t, 2H, J = 6.57 Hz), δ 2.877 (t, 2H, J = 6.68 Hz), δ 3.230 (d, 2H, J=7.66 Hz), δ 4.174 (t, 1H, J = 7.63 Hz,), δ 7.146 – 7.298 (m, 10H). ^{13}C NMR ($CDCl_3$, 75MHz): δ 28.304, 30.063, 45.592, 51.360, 54.558, 80.878, 128.869, 128.283, 128.940, 142.975, 172.112 ppm.

^{1}H NMR ($CDCl_3$, 400 MHz)

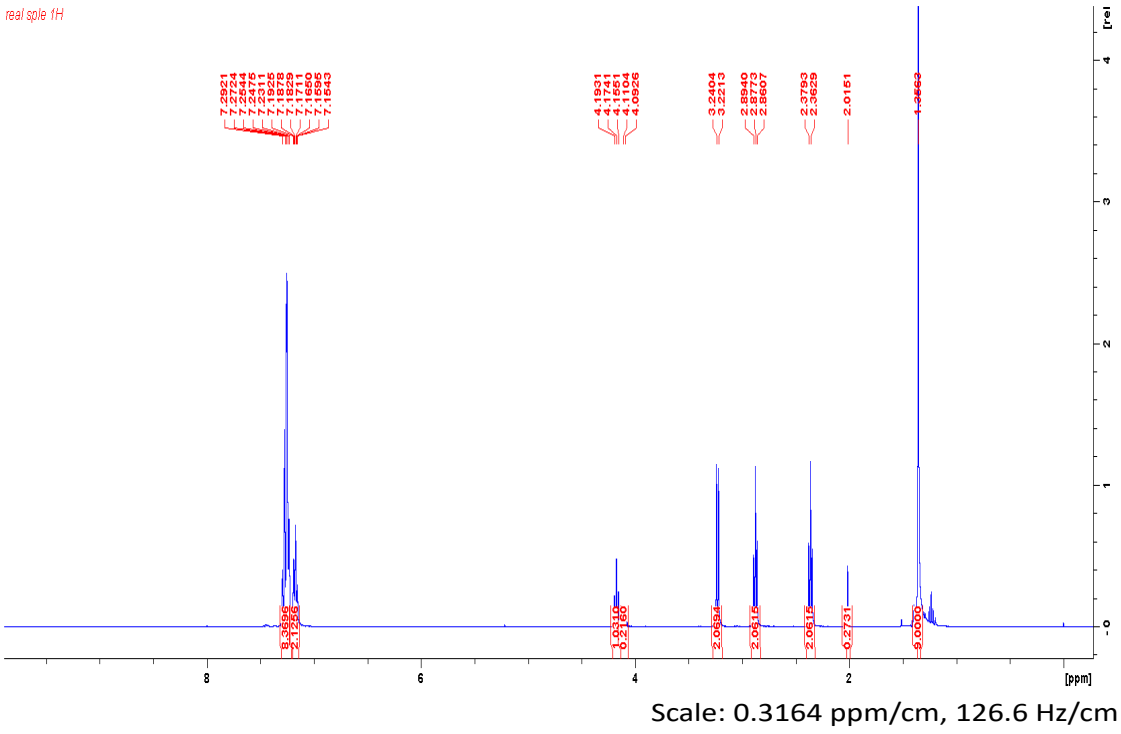

^{13}C NMR ($CDCl_3$, 75MHz)

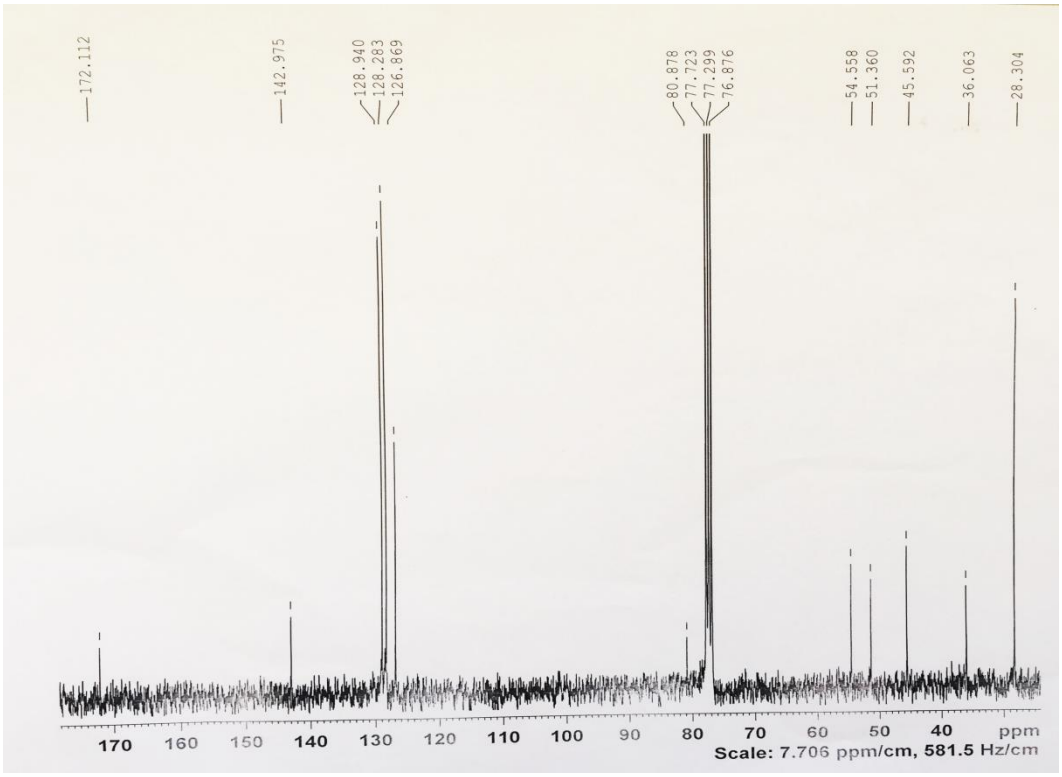

tert-butyl 3-(benzhydrylamino)propanoate (**2**)

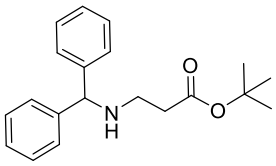

Yield 71%, pale yellow oil. ^1H NMR ($CDCl_3$, 400 MHz): δ 1.582 (s, 9H), δ 2.099 (s_{br}, 1H), δ 2.589 (t, 2H, J = 6.34 Hz), δ 2.950 (t, 2H, J = 6.39 Hz), δ 4.978 (s, 1H), δ 7.338 – 7.518 (m, 10H). ^{13}C NMR ($CDCl_3$, 75 MHz): 28.443, 36.303, 43.976, 67.581, 80.779, 127.281, 127.591, 128.761, 144.219, 172.496 ppm

^{1}H NMR ($CDCl_3$, 400 MHz)

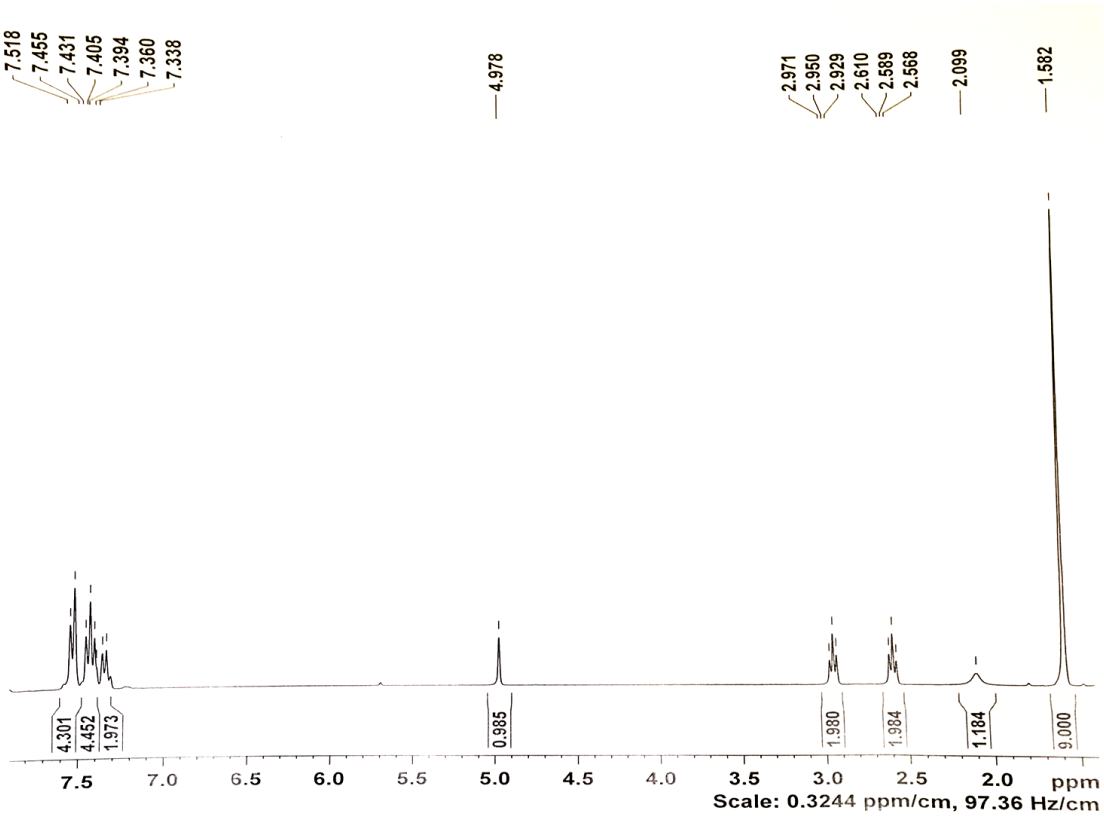

^{13}C NMR ($CDCl_3$, 75MHz)

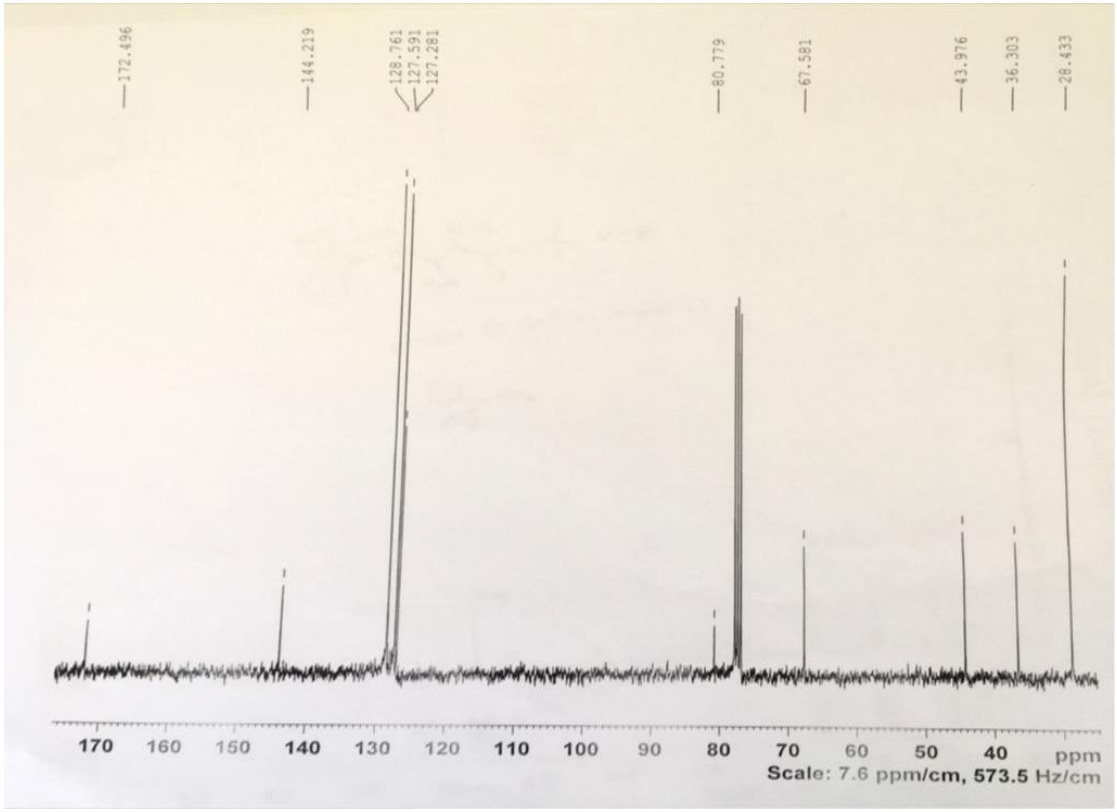

tert-butyl 3-(phenethylamino)propanoate (**3**)

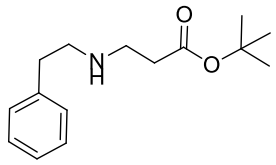

Yield 78%, colorless oil. ^{1}H NMR ($CDCl_3$, 400 MHz): δ 1.411 (s, 9H), δ 2.409 (t, 2H, J = 7.45 Hz), δ 2.75 - 2.912 (m, 6H), δ 7.150 - 7.319 (m, 5H). ^{13}C NMR ($CDCl_3$, 400 MHz): 28.311, 36.127, 36.670, 45.422, 51.300, 80.586, 126.361, 128.686, 128.924, 140.239, 172.218 ppm

^{1}H NMR ($CDCl_3$, 400 MHz)

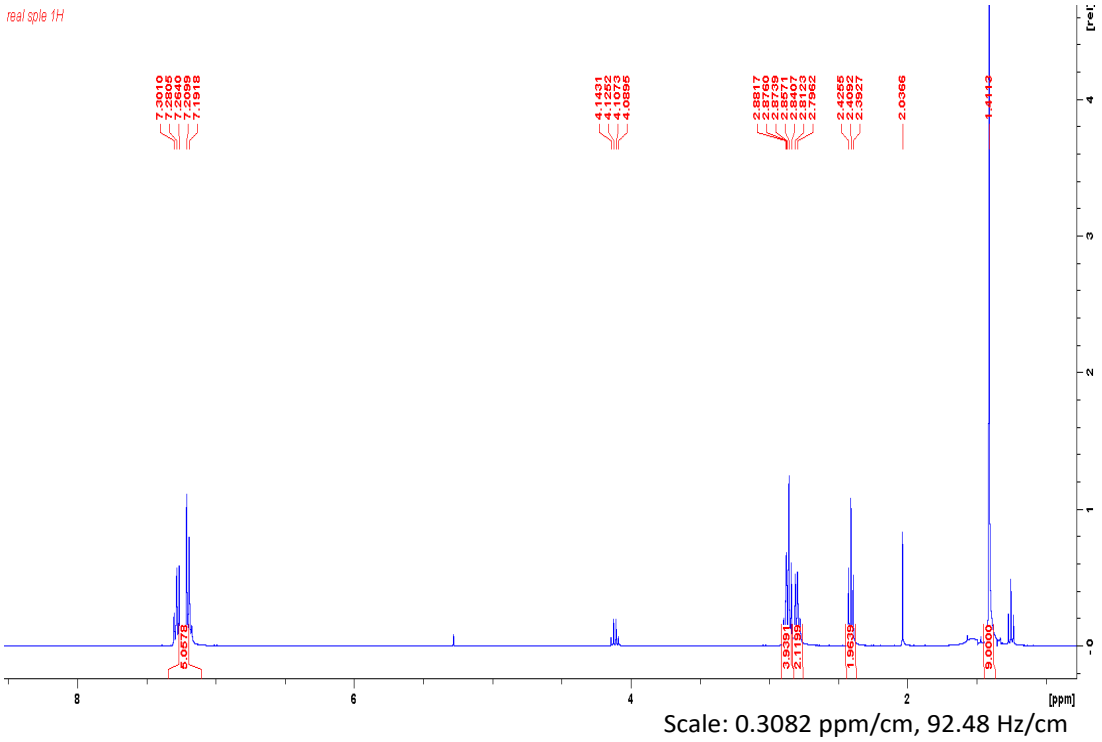

^{13}C NMR ($CDCl_3$, 75MHz)

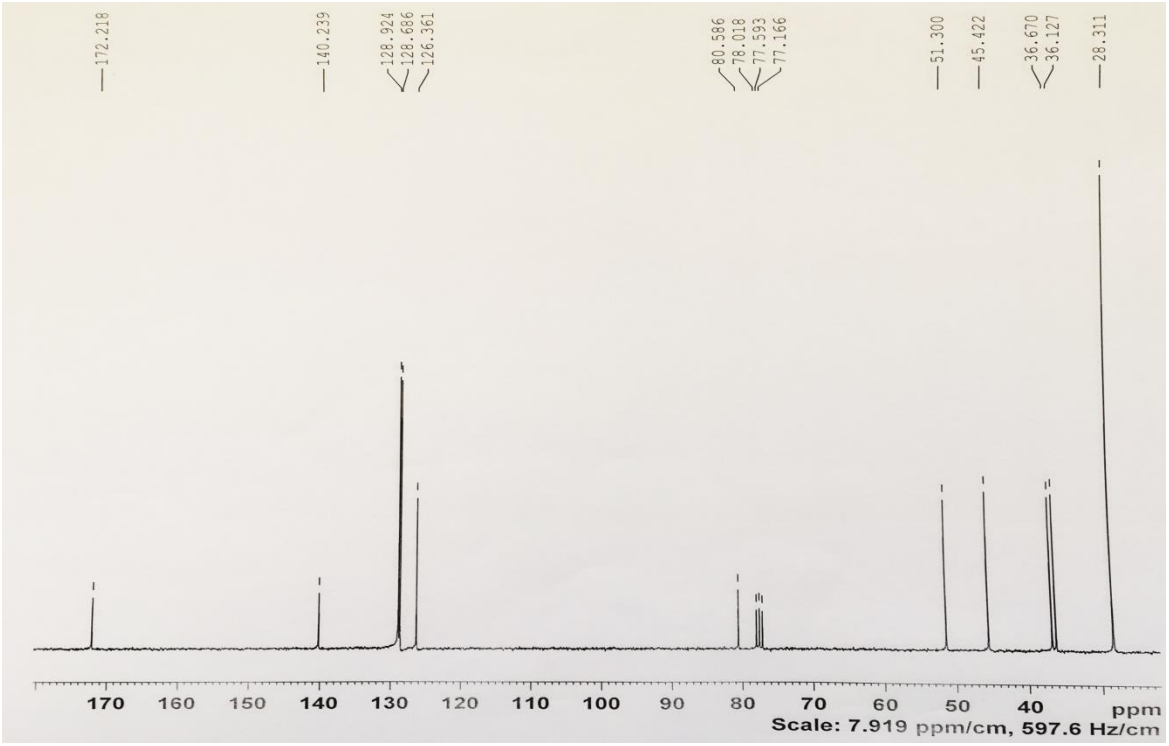

tert-butyl 3-(benzylamino)propanoate (**4**)

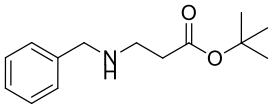

Yield 73%, colorless oil. ^1H NMR ($CDCl_3$, 300 MHz): δ 1.434 (s, 9H), δ 2.441, (t, 2H, J = 6.18 Hz), δ 2.841 (t, 2H, J = 6.18 Hz), δ 3.780 (s, 2H), δ 7.175 -7.4 (m, 5H). ^{13}C NMR ($CDCl_3$, 400 MHz): 28.413, 36.156, 45.033, 54.128, 80.786, 127.220, 128.402, 128.668, 140.487, 172.474 ppm.

^{1}H NMR ($CDCl_3$, 300 MHz)

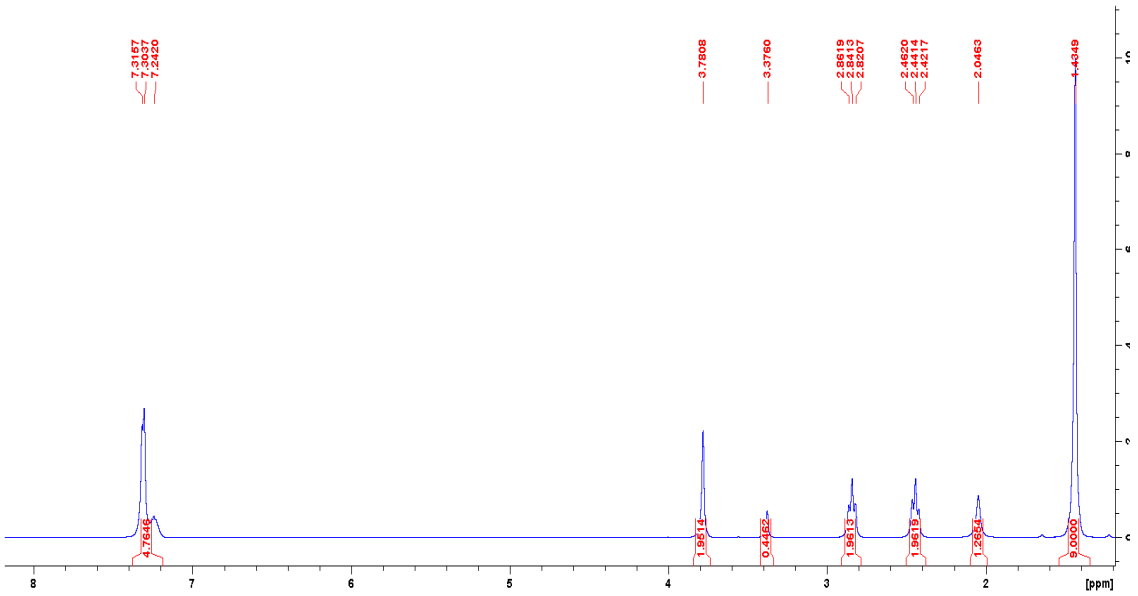

Scale: 0.3086 ppm/cm, 92.6 Hz/cm

^{13}C NMR ($CDCl_3$, 75MHz)

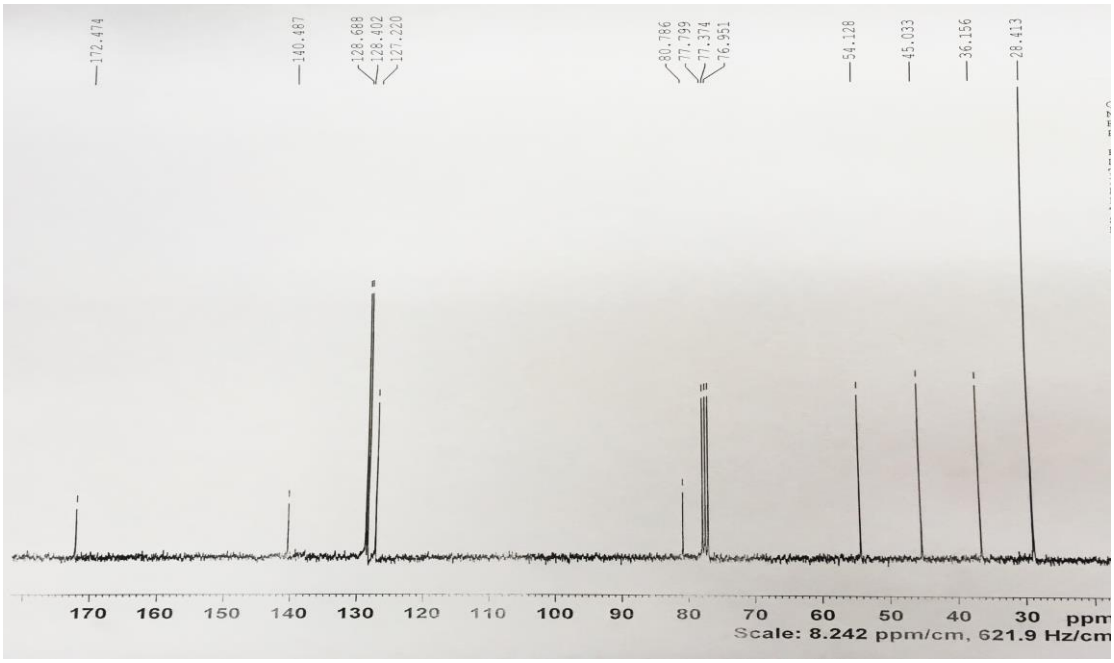

tert-butyl 3-((2-methoxy-1-(naphthalen-1-yl)-2-oxoethyl)amino)propanoate (**5**)

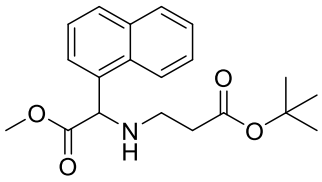

.

Yield 21%, yellow oil. ^{1}H NMR ($CDCl_3$, 300 MHz): δ 1.412 (s, 9H), δ 2.428 (t, 2H, J = 6.43 Hz), δ 2.729-2.980 (m, 2H), δ 3.644 (s, 3H), δ 5.107 (s, 1H), δ 7.374- 7.600 (m, 4H), δ 7.786 (d_{br}, 1H, J = 8.08 Hz), δ 7.837 (d_{br}, 1H, J = 8.08 Hz), δ 8.213 (d_{br}, 1H, J = 8.08 Hz). ^{13}C NMR ($CDCl_3$, 75 MHz): δ 28.396, 36.376, 43.954, 52.557, 62.848, 80.864, δ 123.959, 125.628, 126.741, 129.098, 131.806, 134.403, 172.219,173.925 ppm.

^{1}H NMR ($CDCl_3$, 300 MHz)

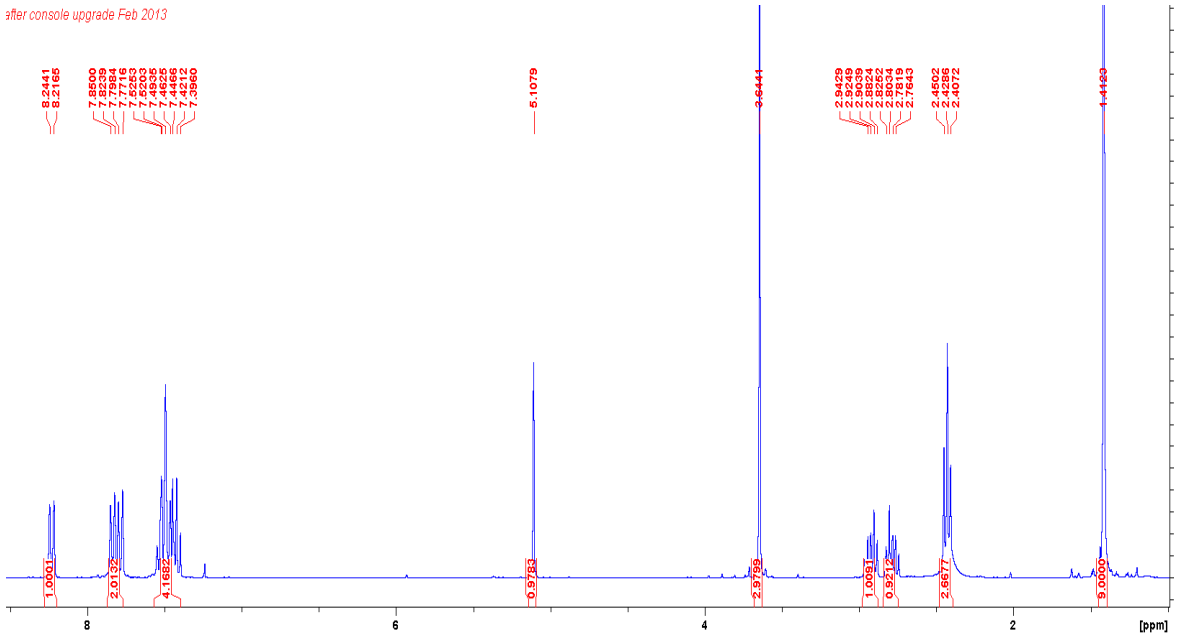

^{13}C NMR ($CDCl_3$, 75MHz)

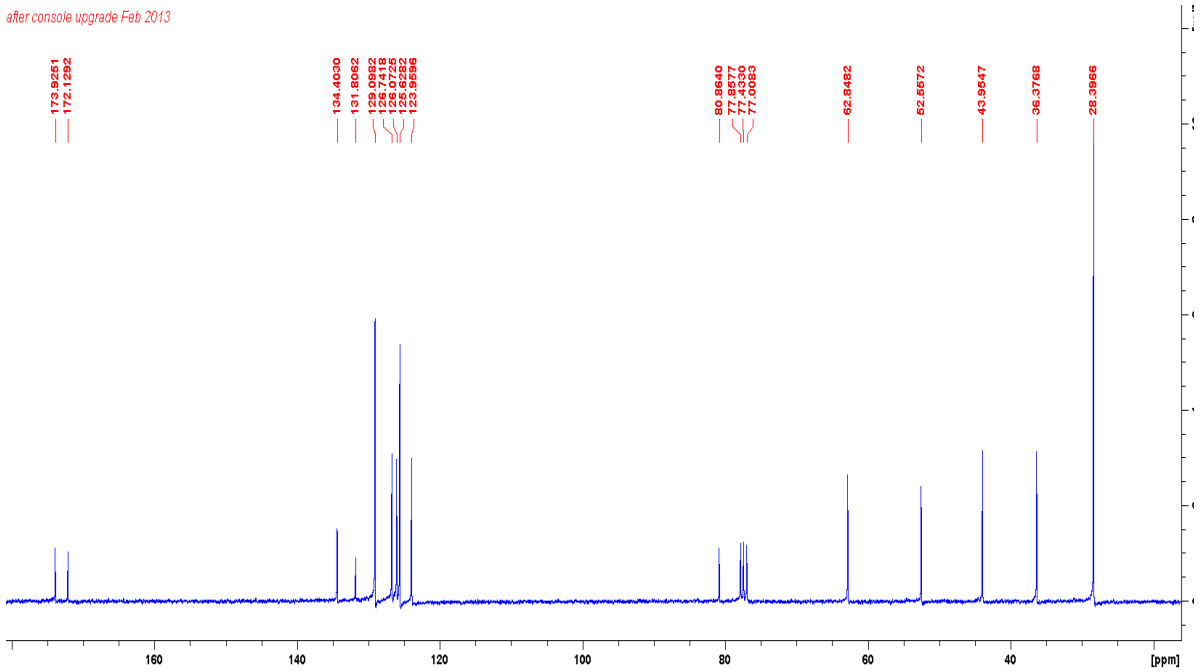

tert-butyl 3-((2-methoxy-1-(naphthalen-2-yl)-2-oxoethyl)amino)propanoate (**6**)

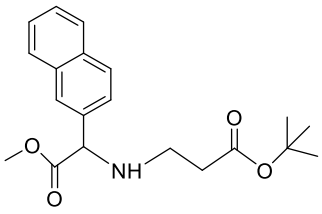

Yield 29%, brown oil. ^1H NMR ($CDCl_3$, 300 MHz): δ 1.452 (s, 9H), δ 2.464 (t, 2H, J = 6.52 Hz), δ 2.710-2.900 (m, 2H), δ 3.689 (s, 3H), δ 4.567 (s, 1H), δ 7.423 - 7.550 (m, 3H,), δ 7.773 - 7.900 (m, 4H). ^{13}C NMR ($CDCl_3$, 75 MHz): δ 27.923, 35.786, 43.031, 52.065, 65.509, 80.384, 123.959, 124.964, 125.962, 126.066, 126.564, 127.481, 127.799, 128.354, 132.994, 133.129, 135.124, 171.614, 172.957 ppm.

^{1}H NMR ($CDCl_3$, 300 MHz)

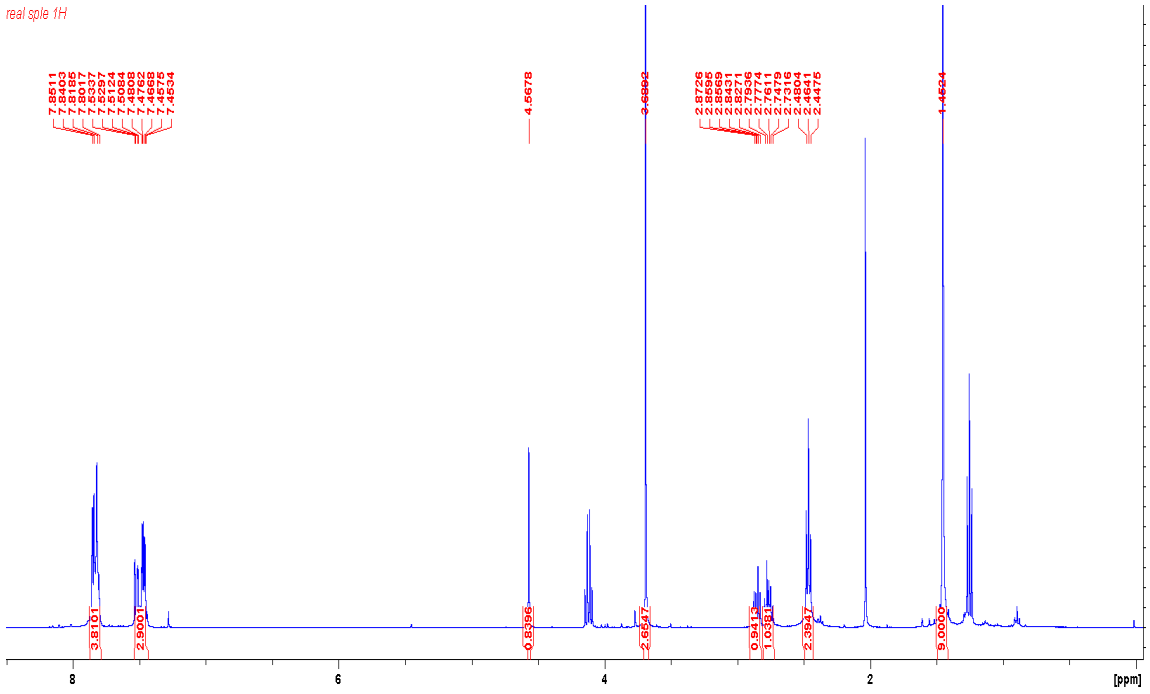

^{13}C NMR ($CDCl_3$, 75MHz)

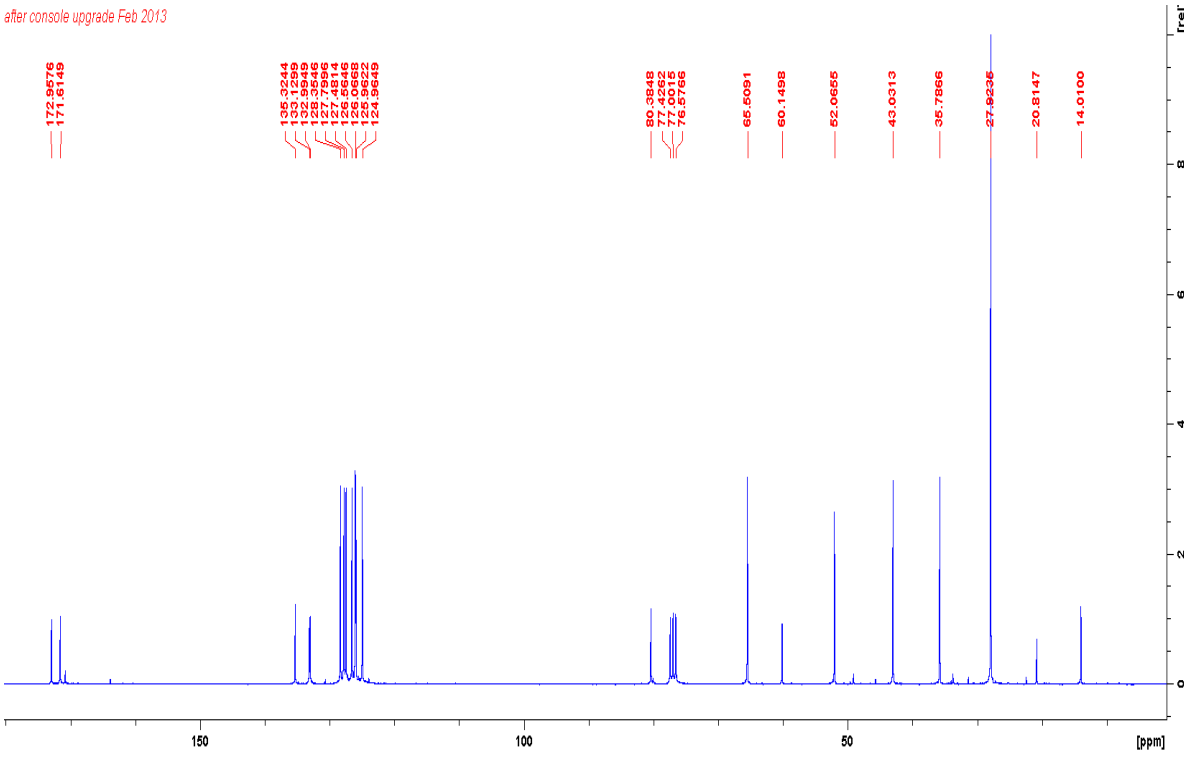

methyl 4-(((3-(tert-butoxy)-3-oxopropyl)amino)methyl)benzoate (**7**)

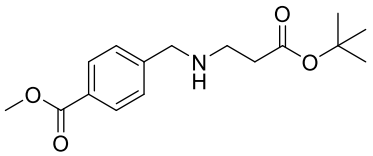

Yield 57%, colorless syrup. ^{1}H NMR ($CDCl_3$, 300 MHz): δ 1.429 (s, 9H), δ 2.432 (t, 2H, J = 6.25 Hz), δ (t, 2H, J = 6.25 Hz), δ 3.835 (s, 2H), δ 3.883 (s, 3H), δ 7.384 (d_{br}, 2H, J = 7.84 Hz), δ 7.974 (d_{br}, 2H, J = 7.84 Hz). ^{13}C NMR ($CDCl_3$, 75 MHz): 28.394, 36.110, 45.061, 52.287, 53.715, 80.853, 128.177, 129.073, 129.992, 145.995, 167.302, 172.405 ppm.

^{1}H NMR ($CDCl_3$, 300 MHz)

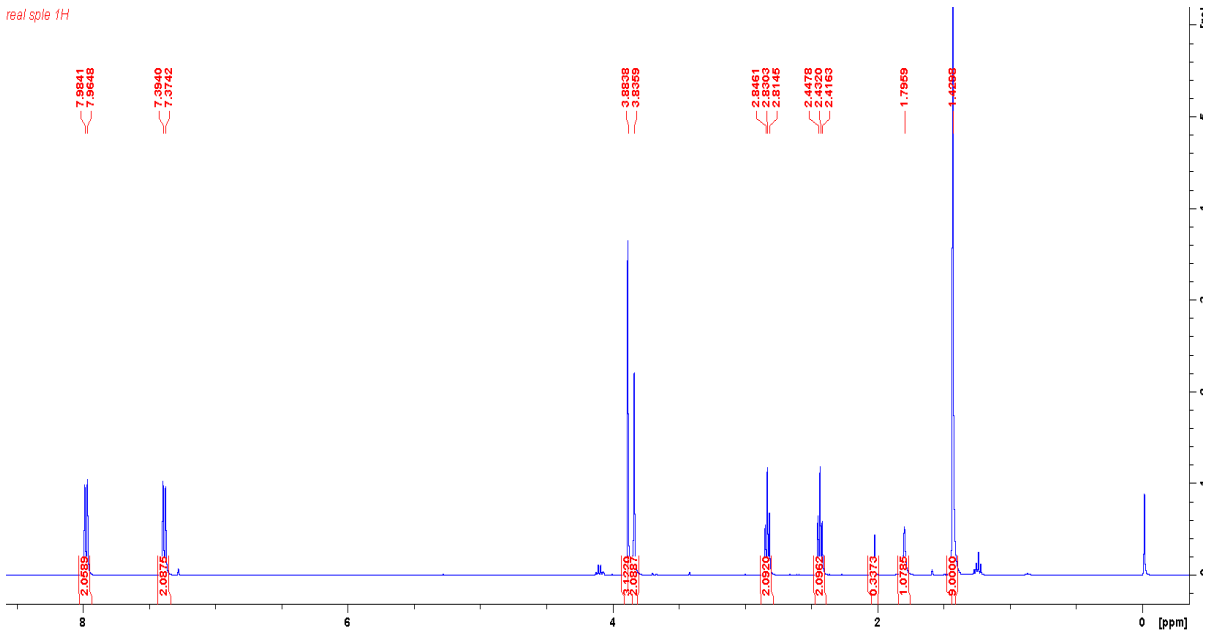

^{13}C NMR ($CDCl_3$, 75MHz)

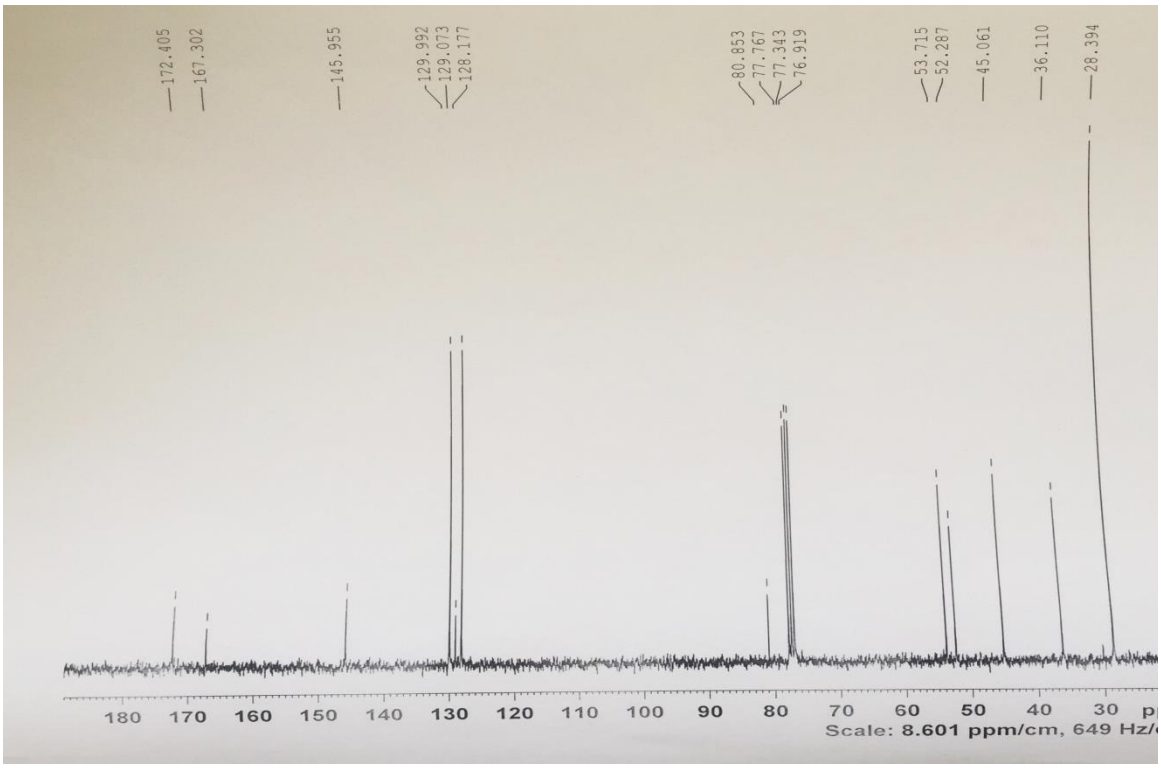

tert-butyl 3-((2-(3,4-dihydroisoquinolin-2(1H)-yl)ethyl)amino)propanoate (**8**)

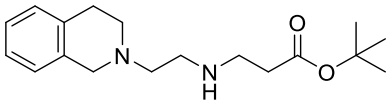

Yield 35%, pale yellow oil. ^{1}H NMR ($CDCl_3$, 400 MHz): δ 1.404 (s, 9H), δ 2.424 (t, 2H, J = 6.62 Hz), δ 2.656 (t, 2H, J = 6.05 Hz), δ 2.736 (t, 2H. J = 5.81 Hz), δ 2.803 (t, 2H, J = 6.05 Hz), δ 2.837 – 2.920 (m, 4H), δ 3.629 (s, 2H), δ 6.966 – 7.035 (m, 1H), δ 7.042 – 7.150 (m, 3H). ^{13}C NMR ($CDCl_3$, 100 MHz): δ 28.038, 29.092, 36.025, 45.422, 46.626, 51.060, 56.109, 57.660, 80.361, 125.503, 126.029, 126.496, 128.554, 134.327, 134.753, 171.975 ppm.

^{1}H NMR ($CDCl_3$, 400 MHz)

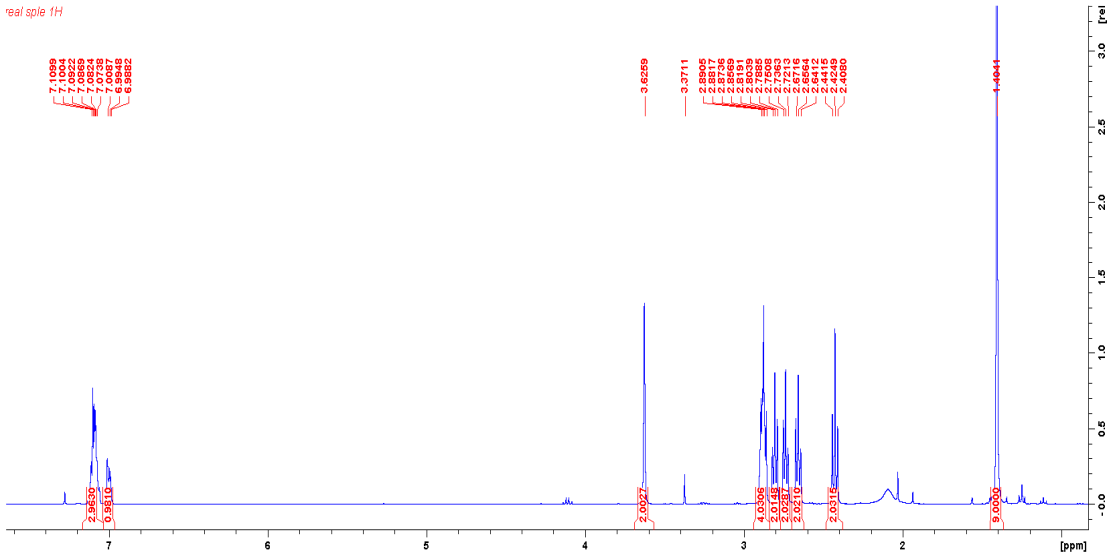

Scale: 0.3087 ppm/cm, 123.5 Hz/cm

^{13}C NMR ($CDCl_3$, 100MHz)

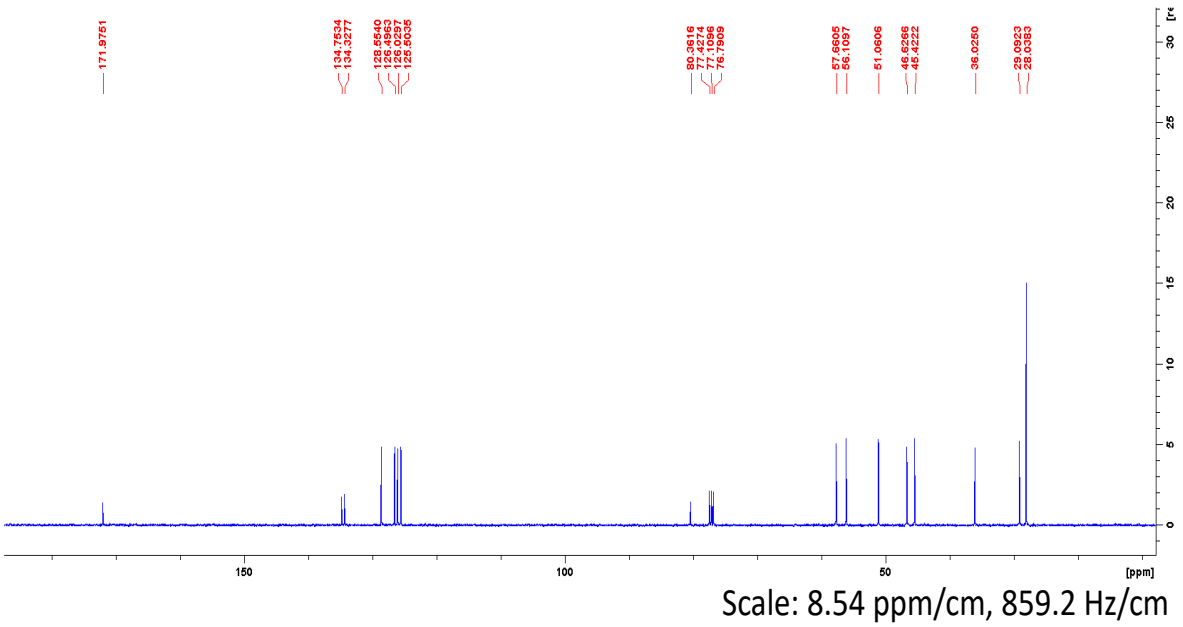

tert-butyl 3-((2-(3-(isobutylcarbamoyl)-3,4-dihydroisoquinolin-2(1H)-yl) ethyl) amino) propanoate (**9**)

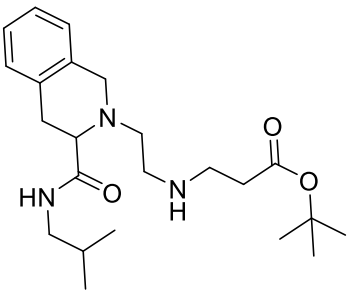

Yield 24%, pale yellow oil. ^1H NMR ($CDCl_3$, 400 MHz): δ 0.742 (dd, J = 3.59 Hz, J = 2.44 Hz, 6H), δ 1.413 (s, 9H), δ 1.435 (s, 2H), δ 2.330-2.501 (m, 3H), δ 2.565 - 2.712 (m, 3H),

δ 2.710 – 2.799 (m, 2H), δ 2.826 (t, J = 6.19 Hz, 2H), δ 2.854 – 2.953 (m, 1H), δ 3.045 (d, J = 6.60 Hz, 2Hz), δ 3.420 (t, 1H, J = 6.93 Hz), δ 3.672 (d, J = 14.89 Hz, 1H), δ 3.894 (d, J = 14.89Hz, 1H), δ 7.00 – 7.180 (m, 4H). ^{13}C NMR ($CDCl_3$, 75 MHz): δ 19.947, 28.0372, 28.473, 28.653, 35.304, 45.099, 46.395, 47.055, 51.888, 54.163, 62.761, 80.657, 126.159, 126.183, 126.907, 128.0149, 172.034, 173.144 ppm.

^{1}H NMR ($CDCl_3$, 400 MHz)

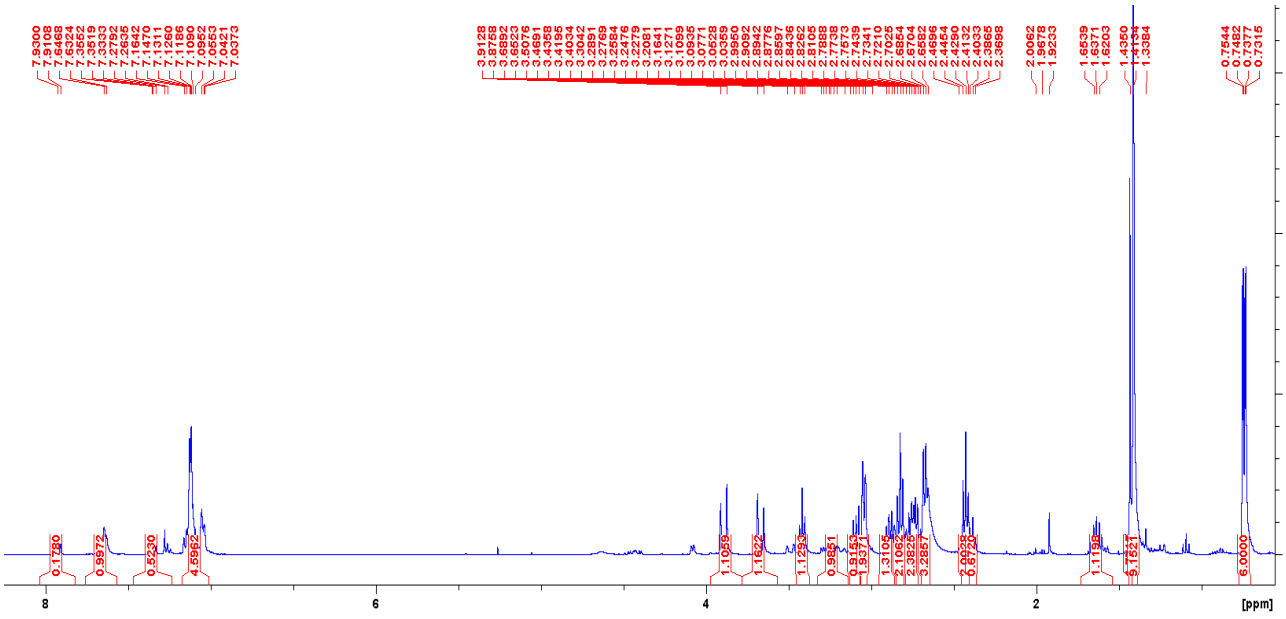

Scale: 0.4177 ppm/cm, 167.1 Hz/cm

^{13}C NMR ($CDCl_3$, 100MHz)

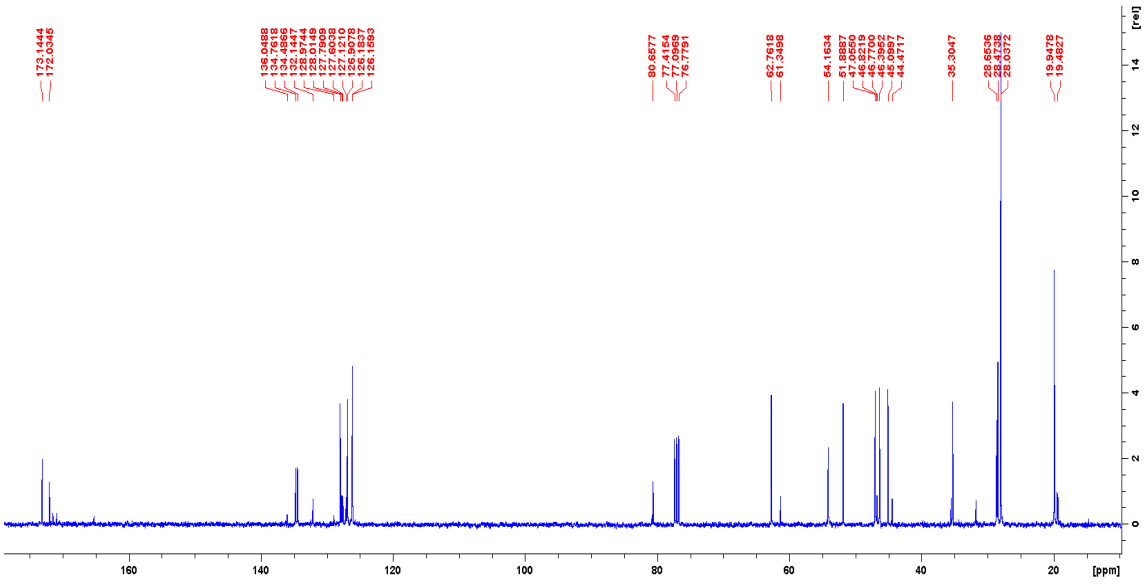

Scale: 8.298 ppm/cm, 834.8 Hz/cm

tert-butyl 3-((2-amino-2-oxoethyl)amino)propanoate (**10**)

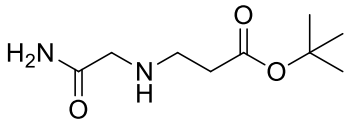

Yield 44%, colorless syrup. ^1H NMR ($CDCl_3$, 300 MHz): δ 1.459 (s, 9H), δ 1.924 (s_{br}, 1H), δ 2.413 (t, J = 6.22 Hz, 2H), δ 2.853 (t, J = 6.06 Hz, 2H), δ 3.275 (s, 2H), δ 6.325 (s_{br}, 1H), δ 7.279 (s_{br}, 1H). ^{13}C NMR ($CDCl_3$, 75 MHz): δ 28.226, 35.543, 45.354, 52.094, 81.189, 172.102, 174.397 ppm.

^{1}H NMR ($CDCl_3$, 300 MHz)

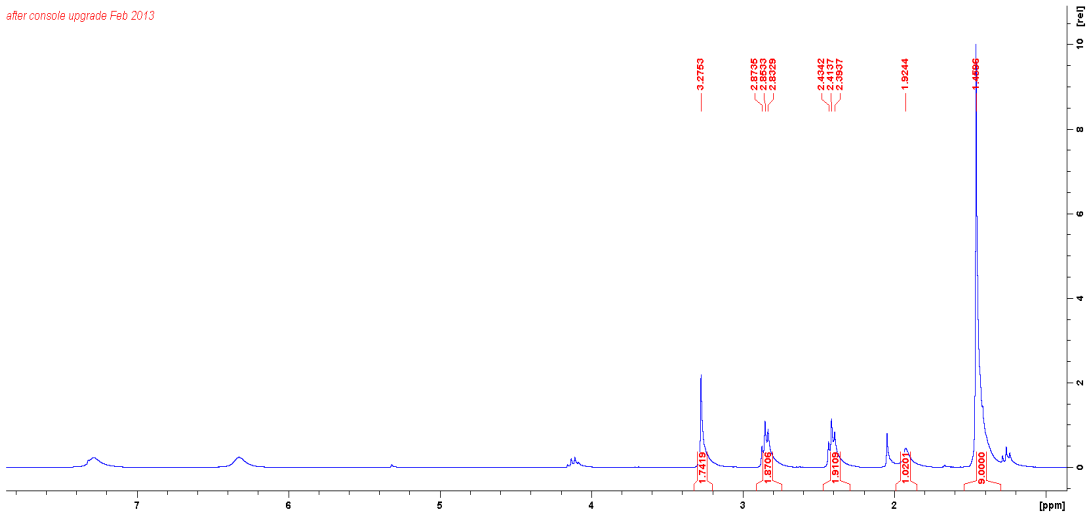

Scale: 0.314 ppm/cm, 94.24 Hz/cm

^{13}C NMR ($CDCl_3$, 75 MHz)

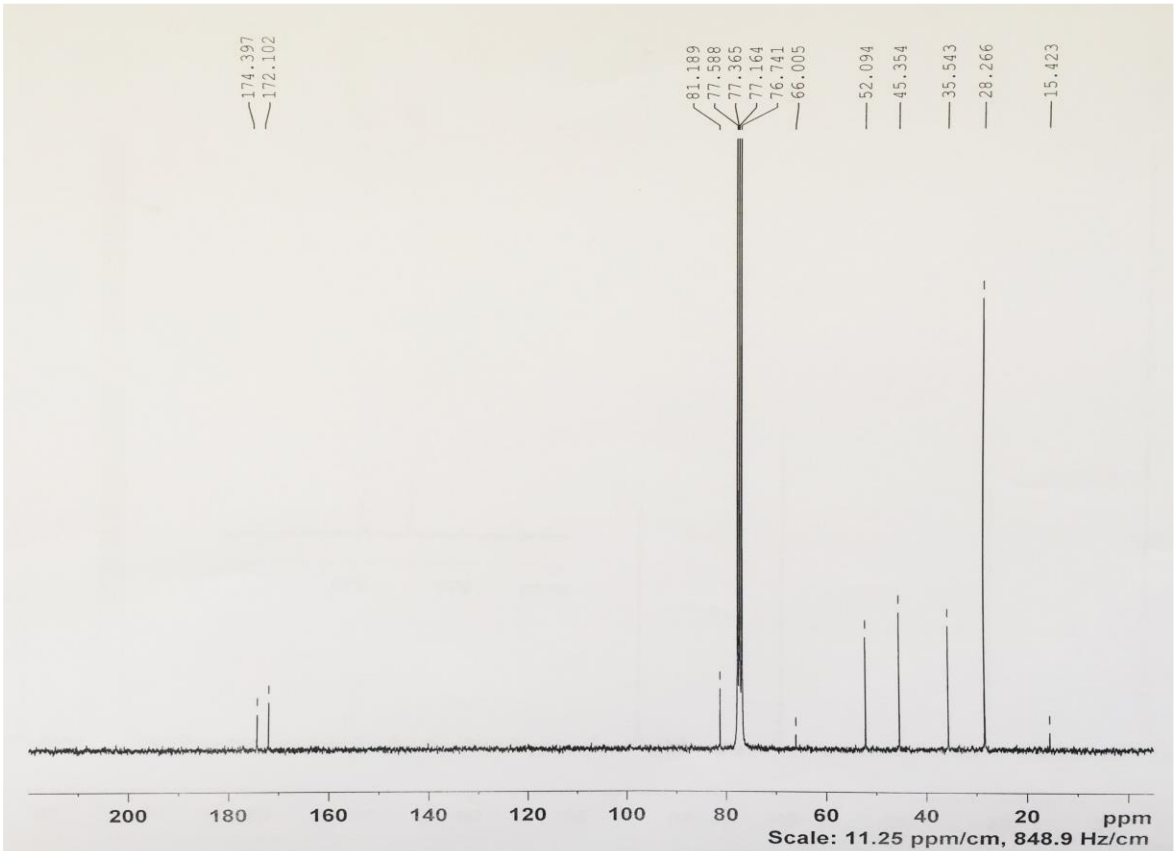

5. Mass spectroscopy analytical data

tert-butyl 3-((2,2-diphenylethyl)amino)propanoate (**1**)

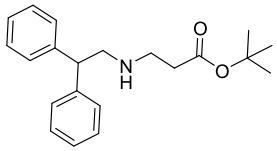

MS Spectrum

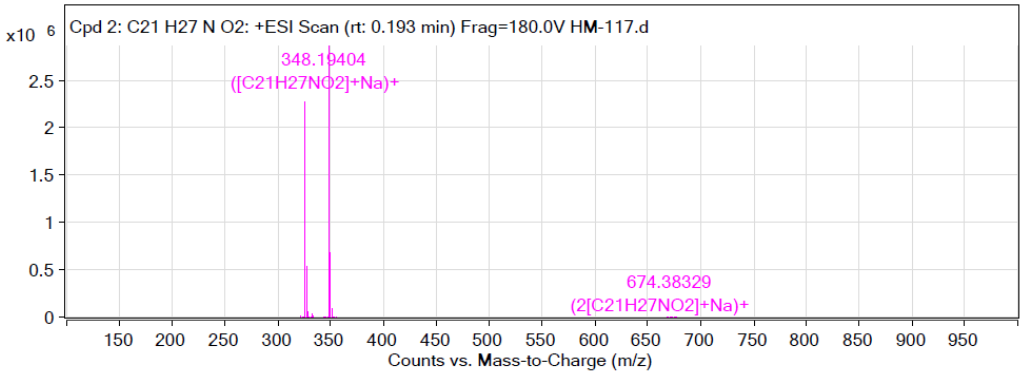

MS Spectrum Peak List

m/z	Calc m/z	Diff(ppm)	z	Abund	Formula	Ion
326.21179	326.21146	-1.04	1	2274720.75	C21H27NO2	(M+H)+
327.21462	327.21475	0.43	1	535768.69	C21H27NO2	(M+H)+
328.21675	328.21773	3	1	66081.25	C21H27NO2	(M+H)+
329.21726	329.22055	10	1	6351.83	C21H27NO2	(M+H)+
348.19404	348.1934	-1.84	1	2862664.5	C21H27NO2	(M+Na)+
349.1966	349.1967	0.27	1	679667.38	C21H27NO2	(M+Na)+
350.19953	350.19968	0.43	1	83553.23	C21H27NO2	(M+Na)+
351.20156	351.20249	2.65	1	7812.88	C21H27NO2	(M+Na)+
673.38927	673.39758	12.34	1	544.67	C21H27NO2	(2M+Na)+
674.38329	674.40088	26.07	1	668.83	C21H27NO2	(2M+Na)+

--- End Of Report ---

tert-butyl 3-(benzhydrylamino)propanoate (**2**)

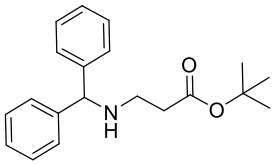

MS Spectrum

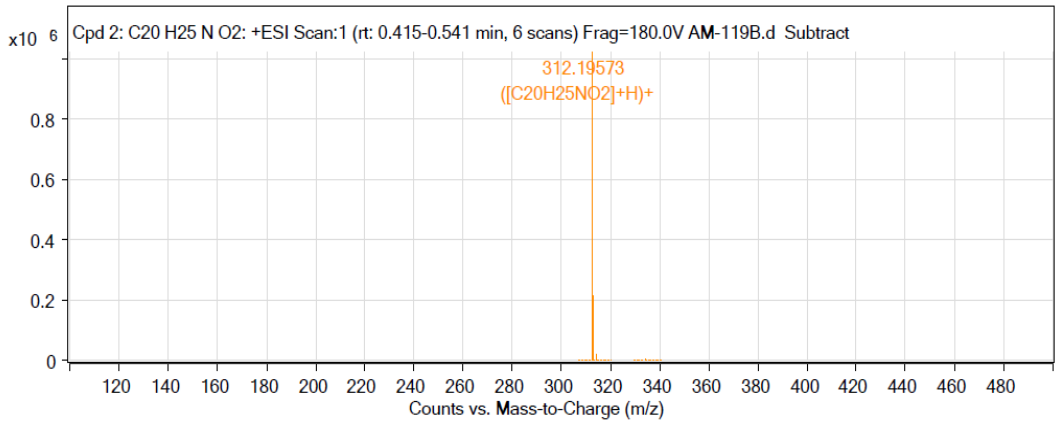

MS Spectrum Peak List

m/z	Calc m/z	Diff(ppm)	z	Abund	Formula	Ion
312.19573	312.19581	0.25	1	1019690.69	C20H25NO2	(M+H)+
313.19901	313.1991	0.29	1	215669.58	C20H25NO2	(M+H)+
314.20241	314.20205	-1.16	1	23741.54	C20H25NO2	(M+H)+
315.20288	315.20483	6.18	1	2830.65	C20H25NO2	(M+H)+
334.17729	334.17775	1.39	1	5208.8	C20H25NO2	(M+Na)+
335.17764	335.18104	10.14	1	1009.97	C20H25NO2	(M+Na)+
336.18043	336.18399	10.59	1	101.27	C20H25NO2	(M+Na)+

--- End Of Report ---

tert-butyl 3-(phenethylamino)propanoate (**3**)

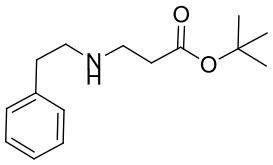

MS Spectrum

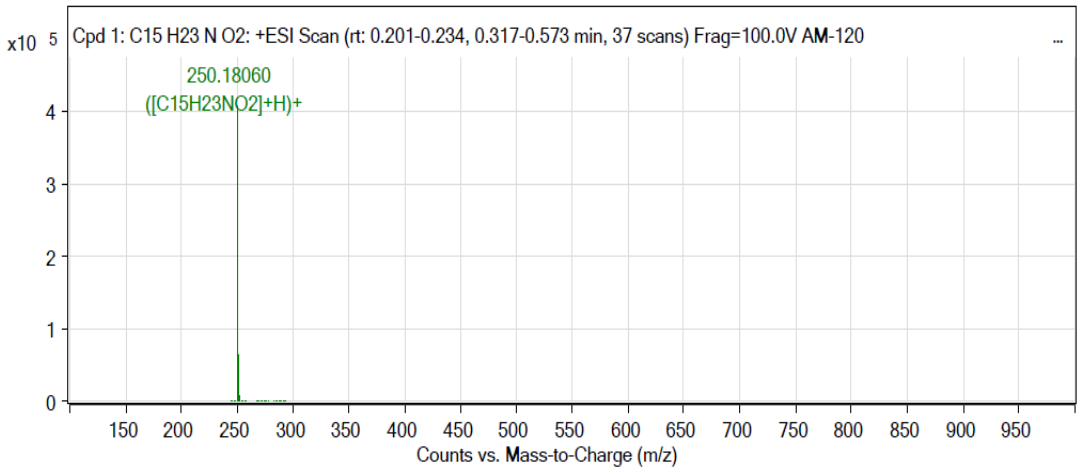

MS Spectrum Peak List

m/z	Calc m/z	Diff(ppm)	z	Abund	Formula	Ion
250.1806	250.18016	-1.76	1	406925.44	C15H23NO2	(M+H)+
251.18407	251.18343	-2.55	1	64045.84	C15H23NO2	(M+H)+
252.18656	252.18616	-1.59	1	6789	C15H23NO2	(M+H)+
253.18855	253.18879	0.92	1	442.21	C15H23NO2	(M+H)+
272.16262	272.1621	-1.9	1	1341.53	C15H23NO2	(M+Na)+
273.167	273.16537	-5.97	1	196.25	C15H23NO2	(M+Na)+
288.13703	288.13604	-3.46	1	77.1	C15H23NO2	(M+K)+

--- End Of Report ---

tert-butyl 3-(benzylamino)propanoate (**4**)

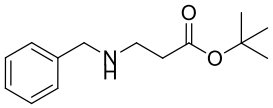

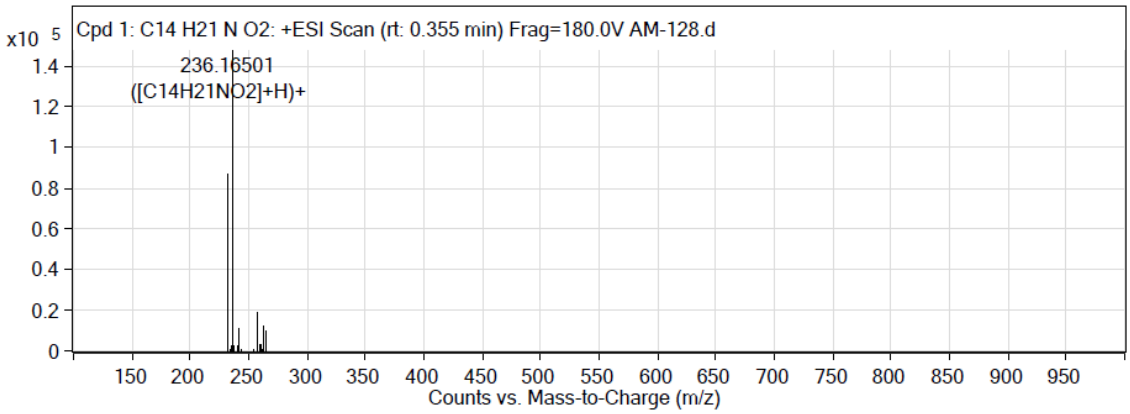

Peak List

m/z	z	Abund	Formula	Ion
236.16501	1	147437.94	C14H21NO2	(M+H)+
237.16827	1	24516.88	C14H21NO2	(M+H)+
238.17096	1	2485.19	C14H21NO2	(M+H)+
258.14657	1	19372.66	C14H21NO2	(M+Na)+
259.14904	1	3161.06	C14H21NO2	(M+Na)+
260.15368	1	667.34	C14H21NO2	(M+Na)+

--- End Of Report ---

tert-butyl 3-((2-methoxy-1-(naphthalen-1-yl)-2-oxoethyl)amino)propanoate (**5**)

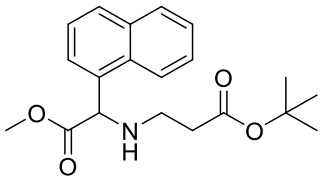

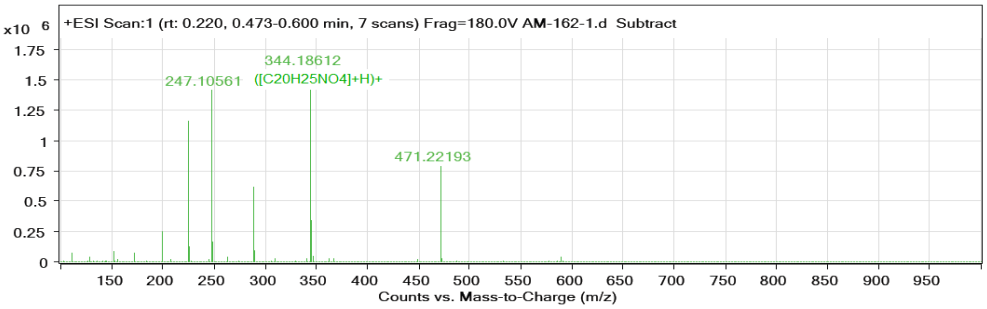

Peak List

m/z	z	Abund
152.03445		90285.15
199.07523		251249.97
225.12364	1	1158127.5
225.19621		620029.81
226.12695	1	128014.73
247.10561	1	1411574.63
248.10883	1	164898.75
288.12293	1	613925
289.12658	1	94706.72
344.18612	1	1585702.75
345.18895	1	343424.69
471.22193	1	785861.56
472.22503	1	192275.16

--- End Of Report ---

tert-butyl 3-((2-methoxy-1-(naphthalen-2-yl)-2-oxoethyl)amino)propanoate (**6**)

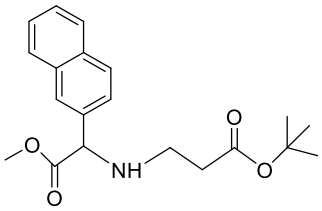

MS Spectrum

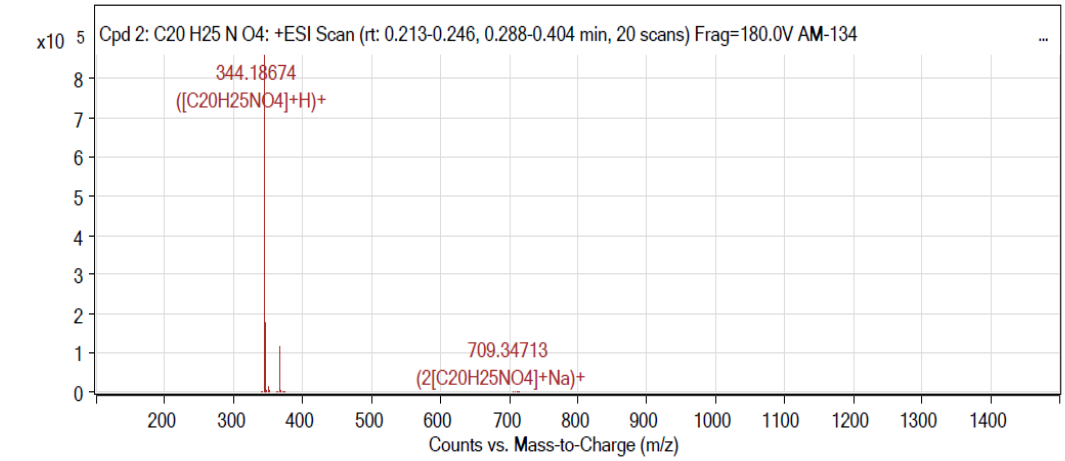

MS Spectrum Peak List

m/z	Calc m/z	Diff(ppm)	z	Abund	Formula	Ion
344.18674	344.18563	-3.2	1	857495.13	C20H25NO4	(M+H)+
345.19019	345.18893	-3.66	1	175699.27	C20H25NO4	(M+H)+
346.19246	346.19163	-2.4	1	22872.15	C20H25NO4	(M+H)+
347.19519	347.19428	-2.64	1	2677.89	C20H25NO4	(M+H)+
366.16852	366.16758	-2.57	1	116307.22	C20H25NO4	(M+Na)+
367.17164	367.17087	-2.07	1	23618.03	C20H25NO4	(M+Na)+
368.17429	368.17357	-1.96	1	3297.91	C20H25NO4	(M+Na)+
369.17861	369.17622	-6.48	1	422.59	C20H25NO4	(M+Na)+
709.34713	709.34594	-1.68	1	472.02	C20H25NO4	(2M+Na)+
710.34953	710.34923	-0.42	1	76.82	C20H25NO4	(2M+Na)+

--- End Of Report ---

methyl 4-(((3-(tert-butoxy)-3-oxopropyl)amino)methyl)benzoate (**7**)

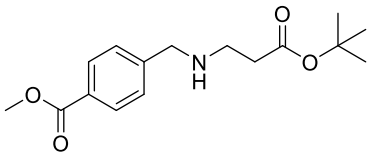

MS Spectrum

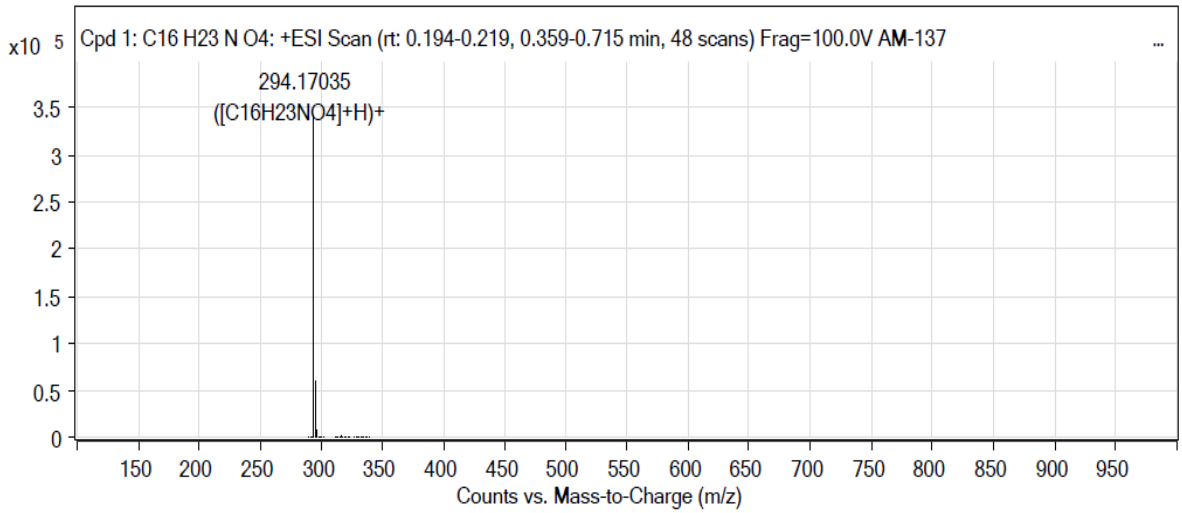

MS Spectrum Peak List

m/z	Calc m/z	Diff(ppm)	z	Abund	Formula	Ion
294.17035	294.16998	-1.26	1	342776.38	C16H23NO4	(M+H)+
295.17363	295.17326	-1.24	1	58629.24	C16H23NO4	(M+H)+
296.17628	296.17574	-1.83	1	7631.56	C16H23NO4	(M+H)+
297.17641	297.17833	6.45	1	689.25	C16H23NO4	(M+H)+
316.1519	316.15193	0.1	1	1509.43	C16H23NO4	(M+Na)+
317.15368	317.15521	4.83	1	320.02	C16H23NO4	(M+Na)+
318.15836	318.15768	-2.15	1	50.94	C16H23NO4	(M+Na)+
332.12604	332.12587	-0.53	1	421.71	C16H23NO4	(M+K)+
333.13132	333.12914	-6.55	1	95.29	C16H23NO4	(M+K)+
334.12099	334.12587	14.61	1	22.01	C16H23NO4	(M+K)+

--- End Of Report ---

tert-butyl 3-((2-(3,4-dihydroisoquinolin-2(1H)-yl)ethyl)amino)propanoate (**8**)

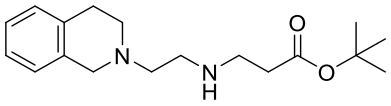

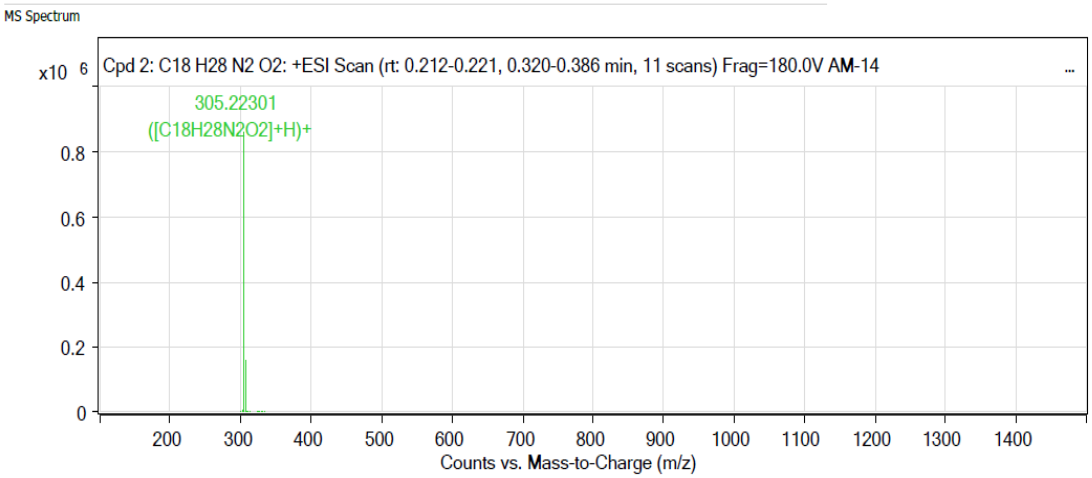

MS Spectrum Peak List

m/z	Calc *m/z*	Diff(ppm)	z	Abund	Formula	Ion
305.22301	305.22235	-2.15	1	863210.69	C18H28N2O2	(M+H)+
306.22618	306.22554	-2.12	1	162855.42	C18H28N2O2	(M+H)+
307.22895	307.22835	-1.95	1	17544.28	C18H28N2O2	(M+H)+
308.23158	308.23102	-1.8	1	1616.55	C18H28N2O2	(M+H)+
327.20358	327.2043	2.2	1	1100.32	C18H28N2O2	(M+Na)+
328.2065	328.20748	2.97	1	217.81	C18H28N2O2	(M+Na)+

--- End Of Report ---

tert-butyl 3-((2-(3-(isobutylcarbamoyl)-3,4-dihydroisoquinolin-2(1H)-yl) ethyl) amino) propanoate (**9**)

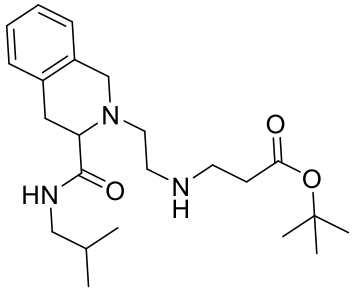

MS Spectrum

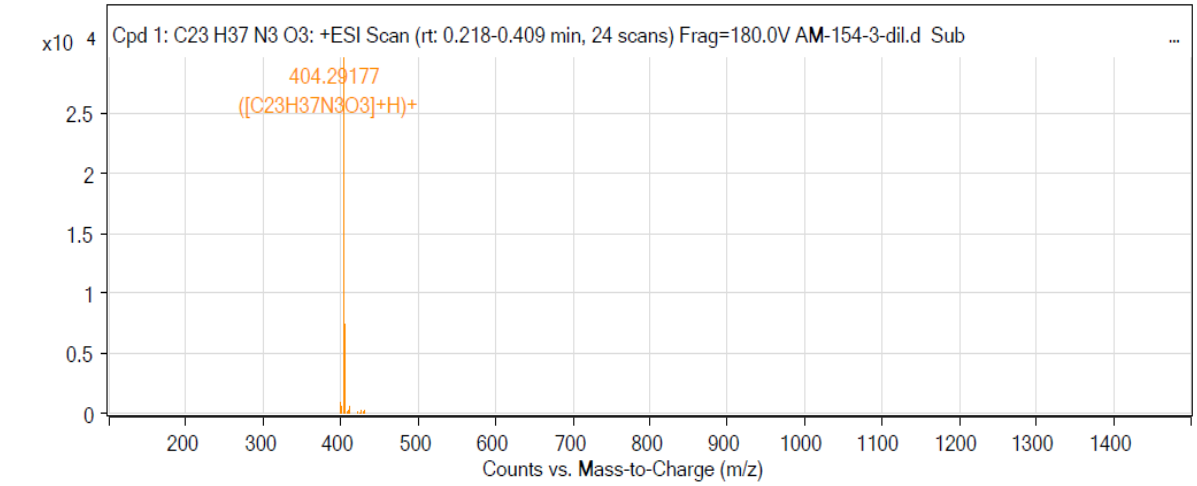

MS Spectrum Peak List

m/z	Calc *m/z*	Diff(ppm)	z	Abund	Formula	Ion
404.29177	404.29077	-2.48	1	29599.73	C23H37N3O3	(M+H)+
405.29504	405.29391	-2.77	1	7514.09	C23H37N3O3	(M+H)+
406.2981	406.29674	-3.35	1	1214.1	C23H37N3O3	(M+H)+
407.29891	407.29943	1.26	1	125.24	C23H37N3O3	(M+H)+
426.27382	426.27271	-2.59	1	320.25	C23H37N3O3	(M+Na)+

--- End Of Report ---

tert-butyl 3-((2-amino-2-oxoethyl)amino)propanoate (**10**)

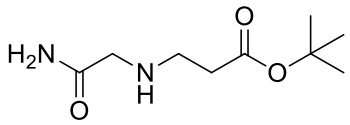

MS Spectrum

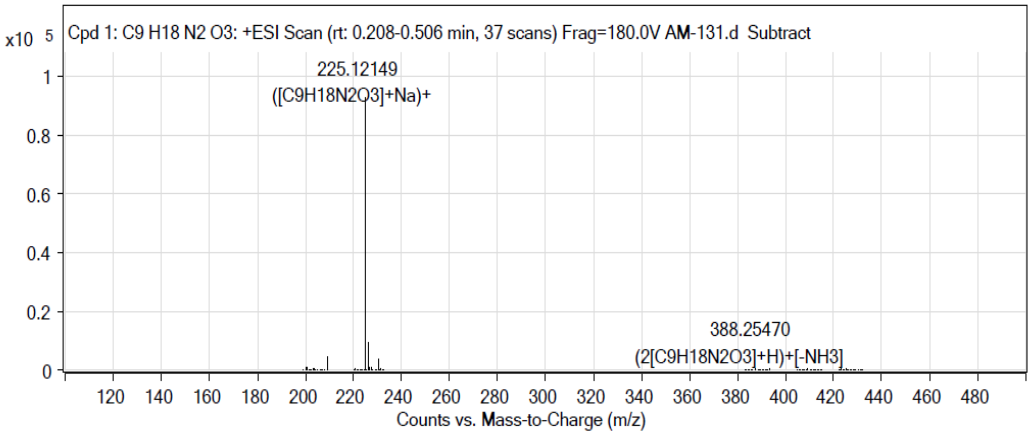

MS Spectrum Peak List

m/z	Calc *m/z*	Diff(ppm)	z	Abund	Formula	Ion
203.13929	203.13902	-1.35	1	811.59	C9H18N2O3	(M+H)+
204.14249	204.14201	-2.31	1	76.64	C9H18N2O3	(M+H)+
225.12149	225.12096	-2.33	1	93037.34	C9H18N2O3	(M+Na)+
226.1246	226.12396	-2.83	1	9679.17	C9H18N2O3	(M+Na)+
227.12686	227.12599	-3.84	1	1078.29	C9H18N2O3	(M+Na)+
228.12832	228.1285	0.81	1	54.78	C9H18N2O3	(M+Na)+
388.2547	388.24421	-27.01	1	215.83	C9H18N2O3	(2M+H)+[-NH3]
410.22591	410.22616	0.61	1	65.83	C9H18N2O3	(2M+Na)+[-NH3]
427.24329	427.25271	22.03	1	78.52	C9H18N2O3	(2M+Na)+

--- End Of Report ---

6. MALDI mass spectra of PAMAM dendrimer

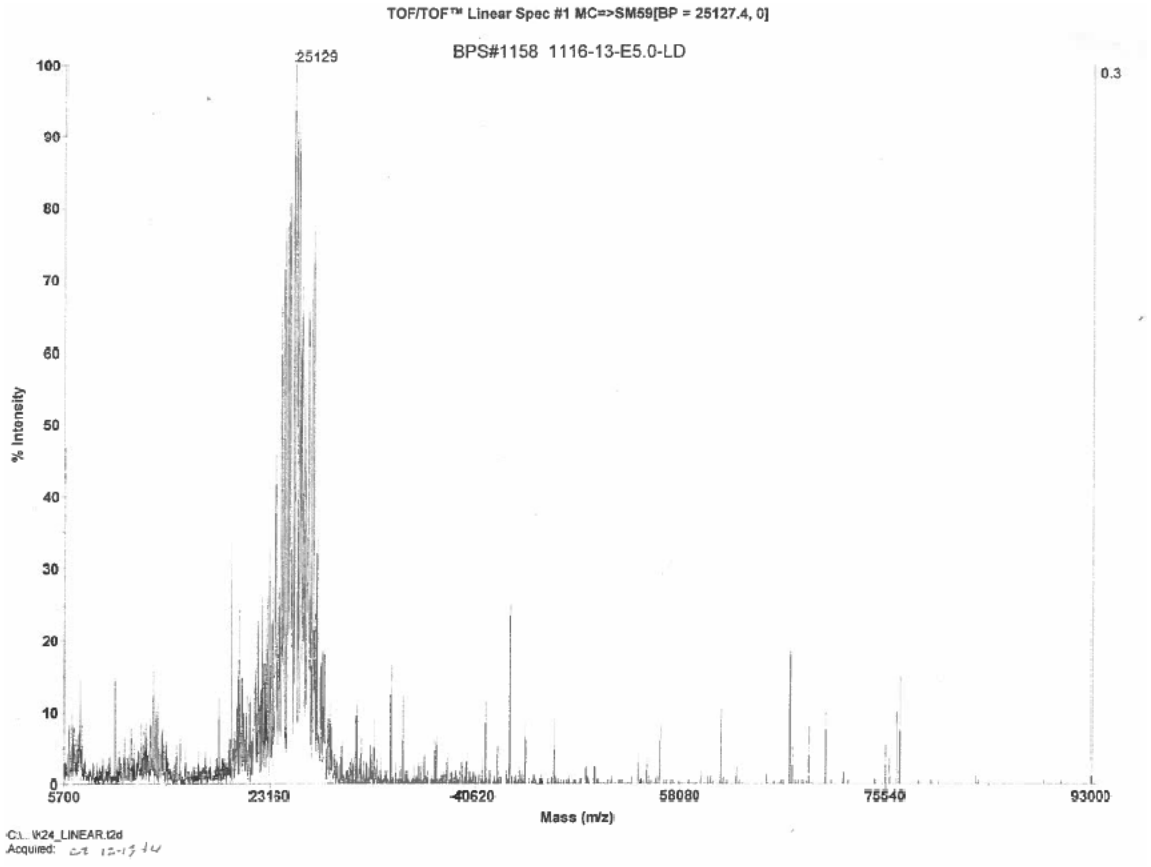

Figure S1. *MALDI mass spectra of PAMAM dendrimer.*

7. HSA-28D characterization

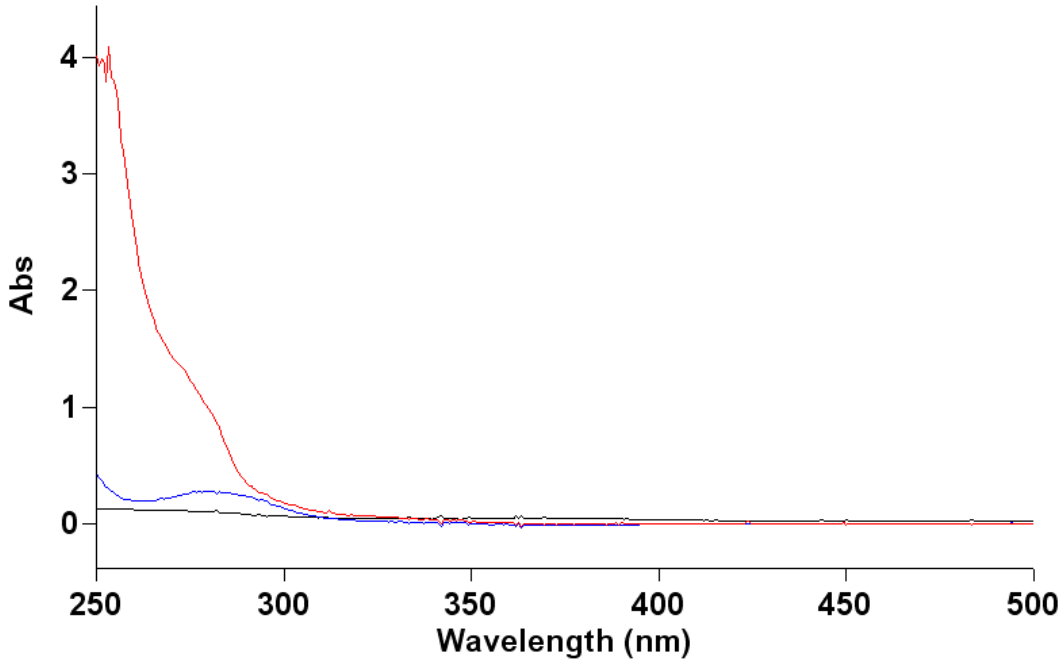

Figure S2. *UV absorption measurement*. "Naked" dendrimer (blue line) and HSA-28D (red line) both at a concentration of 0.175 mM in PBS, pH=7.4, were placed in the plate. UV spectra were recorded at 250-500 nm. The black line is a blank. An Agilent Cary 300 UV-Vis spectrophotometer with a slit of 4nm and a scan speed of 400 nm min^{-1} and a quartz cuvette of 1 cm were used.

8. Estimation of the percentage of dendrimer coating by peptidomimetics

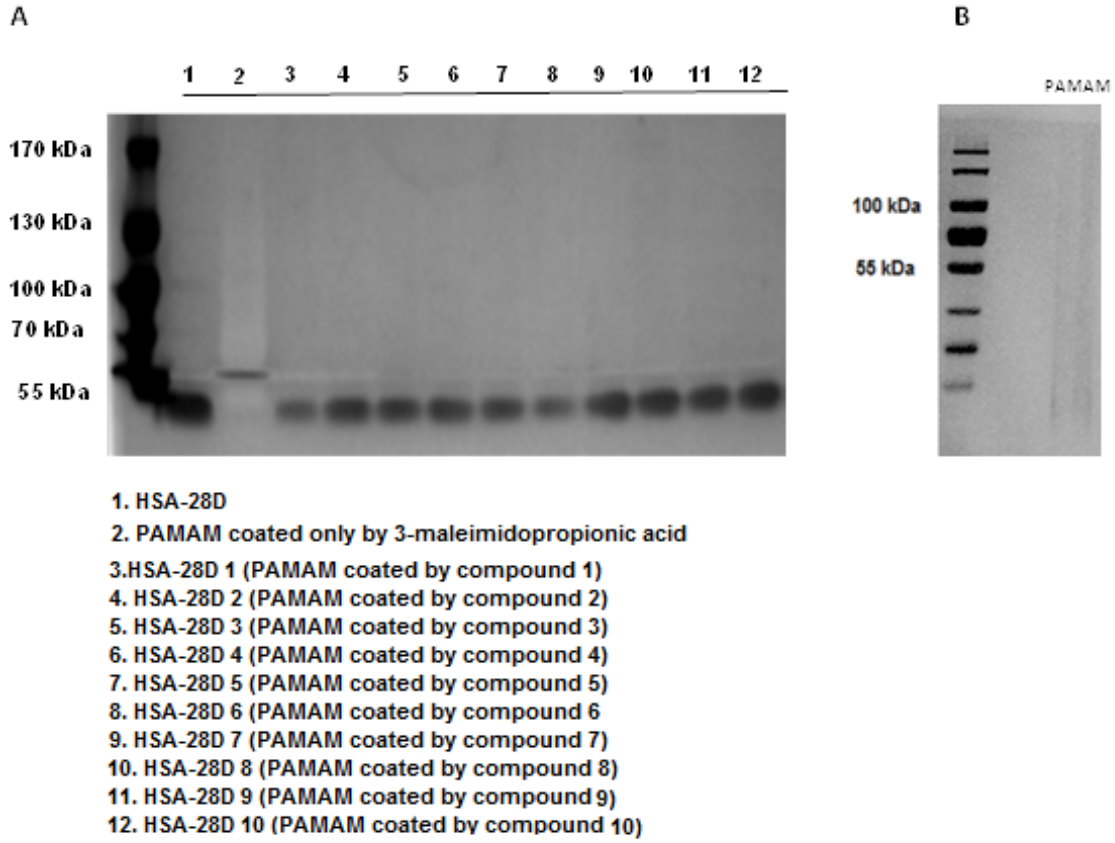

Figure S3. *Gel electrophoresis of coated PAMAMs.* **A.** Samples were loaded to Glycine 6% SDS PAGE gel, run against TTS running buffer, and stained using a silver staining procedure**. B.** Section image of the gel electrophoresis of PAMAM dendrimer, which was conducted as a control for the experiment described above.

9. Lack of biological effect of coated by peptidomimetics PAMAM dendrimer

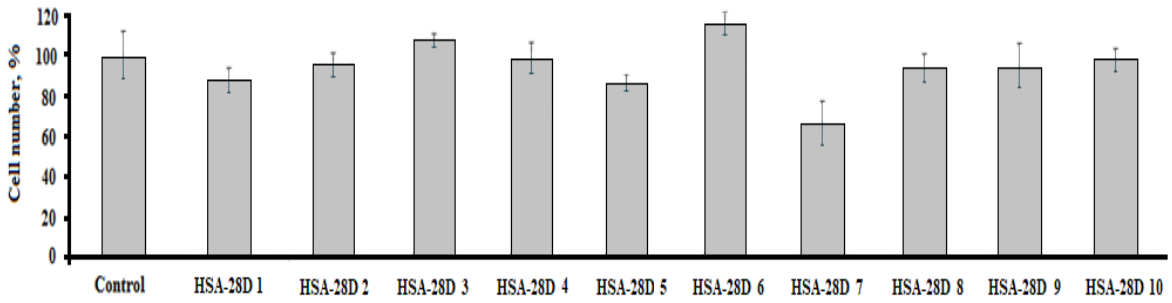

Figure S4. *The effect of coated PAMAMs on the rate of INS-1E cell proliferation*. INS-1E cells were seeded in 24-well plates and incubated for 72h with the medium supplemented with HSA-28D 1-10 ([1-10]-3µg/ml). After the incubation time, the cells were detached by trypsin, colored using Trypan blue and counted. The results are presented as the percentage compared to non-treated cells, n=6, *$p \leq 0.05$. MEAN±SE.